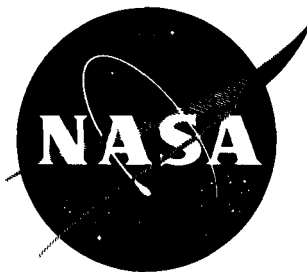


52p.



N 63 18467

CODE-1

TECHNICAL NOTE

D-1929

STATIC AERODYNAMIC CHARACTERISTICS OF
THREE ROCKET-VEHICLE CONFIGURATIONS AT MACH NUMBERS
FROM 1.80 TO 4.63 INCLUDING SOME EFFECTS OF FIN SIZE,
FIN CANT, AND AUXILIARY ROCKET MOTORS

By Dennis E. Fuller and Gerald V. Foster

Langley Research Center
Langley Station, Hampton, Va.

NATIONAL AERONAUTICS AND SPACE ADMINISTRATION
WASHINGTON

July 1963

NATIONAL AERONAUTICS AND SPACE ADMINISTRATION

TECHNICAL NOTE D-1929

STATIC AERODYNAMIC CHARACTERISTICS OF
THREE ROCKET-VEHICLE CONFIGURATIONS AT MACH NUMBERS
FROM 1.80 TO 4.63 INCLUDING SOME EFFECTS OF FIN SIZE,
FIN CANT, AND AUXILIARY ROCKET MOTORS

By Dennis E. Fuller and Gerald V. Foster

SUMMARY

18467

Wind-tunnel tests were made to determine the effects of fin size, fin cant, and auxiliary rocket motors on two three-stage configurations at Mach numbers from 1.80 to 2.86 and the effects of fin size on one two-stage configuration at Mach numbers from 1.80 to 4.63. All tests were performed at a Reynolds number per foot of 2.5×10^6 .

The results indicate that, although there is a significant decrease in stability for the two three-stage models in the test Mach number range, the change in stability level for the model having the same diameter for stages 1 and 2 (model 2) is only about one-half that for the model having stage 2 diameter smaller than that of stage 1 (model 1). In addition, the axial force at an angle of attack of 0° for model 2 is considerably lower than that for model 1 at all test Mach numbers. In general, the variation of the static directional-stability derivative ($C_{n\beta}$) with Mach number for a given configuration is essentially the same as the variation of the static longitudinal-stability derivative with Mach number. Canting the vertical fins 2° on model 1 provided roll effectiveness and some increase in $C_{n\beta}$ throughout the test Mach number range.

INTRODUCTION

The National Aeronautics and Space Administration is currently interested in different types of vehicles for use in various studies such as atmospheric-reentry phenomena and high-altitude probes. Changes in payload requirements and in vehicle performance requirements are often made as a result of these studies. As a continuing effort in vehicle design, an investigation has been made to determine the static stability characteristics of three multistage rocket configurations currently under consideration. Two of the configurations, differing only in second-stage design, were equipped with cruciform fins on the first and

second stages. The third configuration consisted of the second and third stages of one of the three-stage configurations. Tests were also made to determine the effects on aerodynamic characteristics of variation in fin size, fin cant, and number of auxiliary rocket motors attached to the first stage. The results were obtained through a range of Mach numbers from 1.80 to 4.63 at a constant Reynolds number per foot of 2.5×10^6 . The results of wind-tunnel tests of similar configurations may be found in references 1 to 4.

SYMBOLS

The coefficients of forces and moments are referred to the body-axis system. (See fig. 1.) Aerodynamic moments for the three-stage configurations and for the two-stage configuration are presented about points located 12.34 inches and 23.05 inches forward of the first-stage base, respectively, for these configurations. (See figs. 2(a) and 2(d).)

C_A	axial-force coefficient, Axial force/ qS
$C_{A,c}$	chamber axial-force coefficient, Chamber axial force/ qS
$C_{A,o}$	axial-force coefficient at 0° angle of attack
C_l	rolling-moment coefficient, Rolling moment/ qSd
$C_{l,o}$	rolling-moment coefficient at $\beta = 0^\circ$ and $\alpha \approx 0^\circ$
C_m	pitching-moment coefficient, Pitching moment/ qSd
$C_{m\alpha}$	slope of pitching-moment curve through $\alpha = 0^\circ$
C_N	normal-force coefficient, Normal force/ qS
$C_{N\alpha}$	slope of normal-force curve through $\alpha = 0^\circ$
C_n	yawing-moment coefficient, Yawing moment/ qSd
$C_{n\beta}$	slope of yawing-moment curve through $\beta = 0^\circ$
C_Y	side-force coefficient, Side force/ qS
$C_{Y\beta}$	slope of side-force curve through $\beta = 0^\circ$
d	diameter of first stage of test configuration (2.50 in. for three-stage configuration and 4.43 in. for two-stage configuration)

M	free-stream Mach number
q	free-stream dynamic pressure, lb/sq ft
S	cross-sectional area of first stage of test configuration (0.0341 sq ft for three-stage configuration and 0.1071 sq ft for two-stage configuration)
α	angle of attack of model center line, deg
β	angle of sideslip of model center line, deg
δ_I	angle of cant of first-stage fin, in vertical plane, deg
δ_{II}	angle of cant of second-stage fin, in vertical plane, deg

Fin designation:

F ₁	fins for first stage of models 1 and 2, sized to represent full-scale area of 12 square feet
F ₂	fins for first stage of models 1 and 2, sized to represent full-scale area of 10 square feet
F ₃	fins for second stage of models 1 and 2, sized to represent full-scale area of 6 square feet
F ₄	fins for second stage of models 1 and 2, sized to represent full-scale area of 4 square feet
F ₅	fins for first stage of model 3, sized to represent full-scale area of 6 square feet
F ₆	fins for first stage of model 3, sized to represent full-scale area of 4 square feet

APPARATUS AND TESTS

Tunnel

Tests were conducted in both the low and high Mach number test sections of the Langley Unitary Plan wind tunnel which is a variable-pressure, continuous-flow tunnel. The test sections are approximately 4 feet square and 7 feet long. The nozzles leading to the test sections are of the asymmetric sliding-block type, which permit a continuous variation in Mach number from about 1.4 to 2.9 in the low Mach number test section and from about 2.3 to 4.7 in the high Mach number test section.

Models

Dimensional details of the three test vehicles are presented in figure 2 and photographs of the models are presented as figure 3. The two three-stage 1/12.4-scale configurations, hereinafter referred to as models 1 and 2, differed only in size and adaptation of the second stage. The second stage of model 2 had a diameter equal to that of the first stage; whereas, the second stage of model 1 had a diameter essentially one-half that of the adjacent stages and was somewhat longer than the second stage of model 2. The third stage, a cylinder with a slightly larger diameter than the first stage, incorporates a conical nose with a 10° half-angle. The first and second stages of models 1 and 2 were equipped with identical cruciform stabilizing surfaces oriented on a horizontal and a vertical plane. Two sizes of fins were tested for both stages of the models. The first-stage fins were trapezoidal in planform with a hexagonal section. One set of these fins sized to represent a full-scale area of 12 square feet is hereinafter referred to as F_1 . A smaller set of fins (10 square feet full scale and noted by F_2) was constructed by decreasing the span of fins F_1 . The second-stage fins were of clipped delta planform with an 8° total angle wedge section. These fins, hereinafter referred to as F_3 and F_4 , were sized to represent full-scale areas of 6 square feet and 4 square feet, respectively. The vertical fins for both the first and second stages could be canted 2° to produce positive roll. Details of these fins are shown in figure 2(b). The first stage of models 1 and 2 was equipped with two auxiliary rockets for the majority of these tests; also, the effects of an additional two rockets on model 2 were determined.

The two-stage configuration, hereinafter referred to as model 3, is the same as the second and third stages of model 2, including the two sets of test fins F_5 and F_6 , except for model scale (see fig. 2(d)) which was increased to one-seventh.

Test Conditions

The test conditions for the investigation were as follows:

Model	Mach number	Stagnation temperature, $^\circ\text{F}$	Stagnation pressure, lb/sq in. abs	Reynolds number per foot
1 and 2	1.80	125	10.02	2.5×10^6
1 and 2	2.50	150	14.71	2.5
1 and 2	2.86	150	17.76	2.5
3	2.96	150	18.77	2.5
3	3.95	175	33.29	2.5
3	4.63	175	45.54	2.5

All configurations were tested through an angle-of-attack range from approximately -6° to 6° at an angle of sideslip of 0° and through an angle-of-sideslip range from about -4° to 4° at angles of attack of about -4° , 0° , and 4° . The stagnation dewpoint was maintained at -30° F in order to avoid condensation effects.

In order to obtain turbulent flow over the model, a 1/8-inch-wide strip of 0.012-inch-diameter carborundum grains was affixed around the model 1 inch behind the nose.

Measurements

Aerodynamic forces and moments were measured by means of a six-component electrical strain-gage balance housed within the model. The balance, in turn, was rigidly fastened to a sting support and thence to the tunnel support system. The balance-chamber pressure was measured for each model and test condition.

Accuracy

The accuracy of the individual measured quantities, based on calibrations and repeatability of data, is estimated to be within the following limits:

Models 1 and 2

C_A	± 0.005
$C_{A,c}$	± 0.007
C_l	± 0.008
C_m	± 0.033
C_n	± 0.033
C_N	± 0.037
C_Y	± 0.038

Model 3

C_A	± 0.008
$C_{A,c}$	± 0.007
C_m	± 0.003
C_N	± 0.006

Angles of attack and sideslip are accurate within $\pm 0.10^{\circ}$. The Mach number accuracy for the range from $M = 1.80$ to $M = 2.96$ is estimated to be within ± 0.015 and for the range from $M = 3.95$ to $M = 4.63$, within ± 0.050 .

Corrections

Angles of attack were corrected for tunnel-flow angularity and for deflection of balance and sting support as a result of aerodynamic loads. The axial-force data were adjusted to correspond to free-stream static conditions in the balance chamber. Typical values of chamber axial-force coefficient are presented in figure 4.

PRESENTATION OF RESULTS

The results of this investigation are presented in the following figures:

	Figure
Longitudinal aerodynamic characteristics:	
Effect of Mach number variation and change in fin size and cant for model 1	5
Effect of Mach number variation and number of auxiliary rocket motors for model 2	6, 7
Effect of Mach number variation and change in fin size for model 3 . .	8
Lateral aerodynamic characteristics:	
Effect of Mach number variation and change in fin size and cant for model 1	9
Effect of Mach number variation and number of auxiliary rocket motors for model 2	10, 11
Summary of longitudinal aerodynamic characteristics	12
Summary of lateral aerodynamic characteristics	13

RESULTS AND DISCUSSION

The basic aerodynamic characteristics for the three test vehicles are presented in figures 5 to 11 and are summarized in figures 12 and 13. It should be pointed out that the moment data are presented about a point corresponding to the balance pitch center for each model. As a consequence these data do not reflect the stability level that would be obtained with a more realistic center-of-gravity location.

The results in figure 12(a) show a significant decrease in stability for model 1 with increase in Mach number from 1.80 to 2.86 when fins F_1 and F_3 are fixed to the first and second stages, respectively. The decrease in stability for model 2, while significant, is only about one-half that for model 1 in this Mach number range. The difference in the effect of Mach number on the stability of these models is associated with a forward shift in center of pressure arising

from the longer second stage of model 1. There is little difference in $C_{N\alpha}$ for the two configurations; however, the axial force at $\alpha = 0^\circ$ is considerably lower for model 2 than for model 1 at all test Mach numbers. This higher $C_{A,0}$ for model 1 is probably associated with the boattailing of the third stage and the flare of the first stage. As would be expected, a decrease in the size of the fins of model 1 (fig. 12(b)) results in a decrease in $C_{A,0}$ and $C_{N\alpha}$ with an associated change in stability level at a given Mach number. A decrease in fin size for model 3 (second and third stages of model 2) results in a decrease in $C_{A,0}$, $C_{N\alpha}$, and stability level (fig. 12(e)). The data of figure 12(d) indicate that the addition of two more auxiliary rocket motors to model 2 increases $C_{A,0}$ substantially but has little effect on $C_{m\alpha}$ or $C_{N\alpha}$.

In general, the variation of $C_{n\beta}$ for a given configuration with Mach number is essentially the same as that shown by $C_{m\alpha}$. This would be expected since the models are essentially symmetrical about the horizontal and vertical planes. The result of canting the vertical fins 2° on the first and second stages of model 1 (fig. 13(c)) indicated that, although the roll effectiveness of the vertical fins decreased with Mach number, the fins remained effective and provided some increase in $C_{n\beta}$ throughout the test Mach number range.

CONCLUSIONS

Results of tests of three rocket-vehicle configurations with variations in fin size, fin cant, and auxiliary rocket motors at Mach numbers from 1.80 to 4.63 lead to the following conclusions:

1. The change in stability level with increase in Mach number for the model having an equal diameter for stages 1 and 2 (model 2) is only about one-half that for the model having stage 2 diameter smaller than stage 1 (model 1).

2. Canting the vertical fins 2° on model 1 provided roll effectiveness throughout the test Mach number range.

Langley Research Center,
National Aeronautics and Space Administration,
Langley Station, Hampton, Va., May 6, 1963.

REFERENCES

1. Brown, Clarence A., Jr., and Carraway, Ausley B.: Static Aerodynamic Characteristics of a Two-Stage and a Three-Stage Rocket Vehicle at Mach Numbers From 1.47 to 4.63. NASA TN D-1232, 1962.
2. Carraway, Ausley B., Edwards, Frederick G., and Keating, Jean C.: Investigation of the Static Stability Characteristics of Two Stages of a Three-Stage Missile at a Mach Number of 4.00. NASA TN D-651, 1961.
3. Gregory, Donald T., and Carraway, Ausley B.: Investigation of the Static Longitudinal Stability and Roll Characteristics of a Three-Stage Missile Configuration at Mach Numbers From 1.77 to 2.87. NASA TM X-124, 1959.
4. Robinson, Ross B.: Effects of Body and Fin Deflections on the Aerodynamic Characteristics in Pitch of a 0.065-Scale Model of a Four-Stage Rocket Configuration at Mach Numbers of 1.41 and 1.82. NASA TN D-37, 1959.

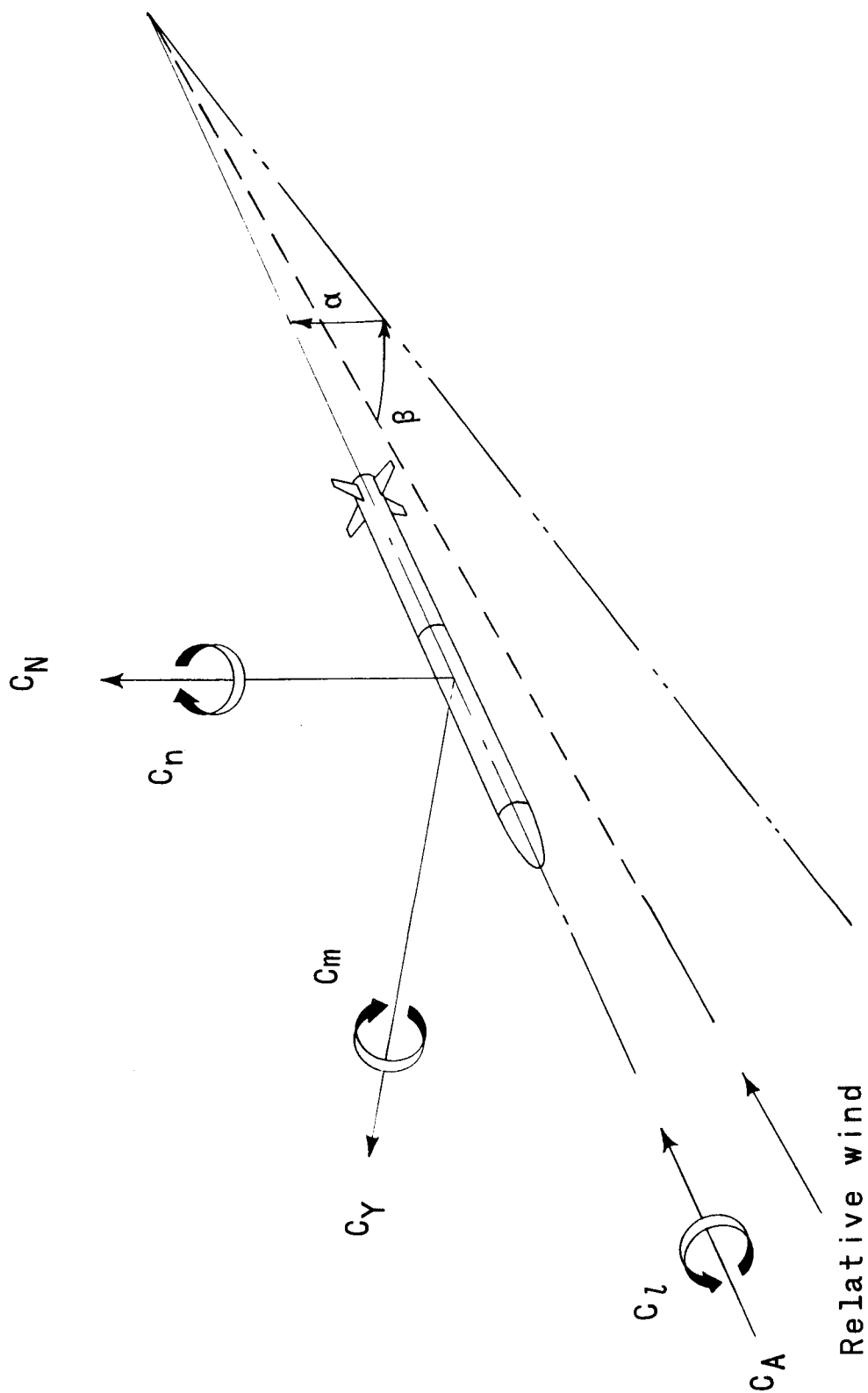
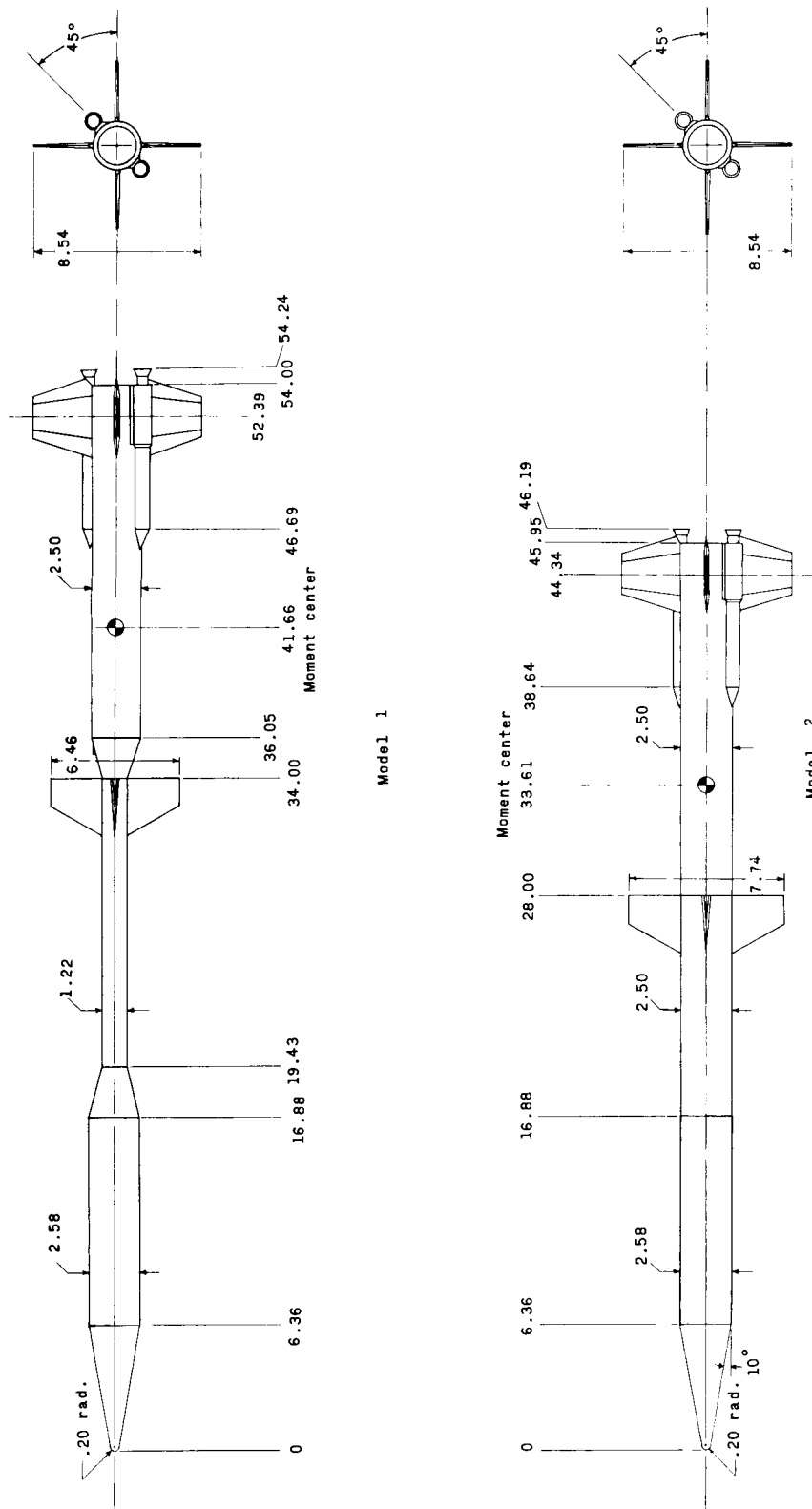
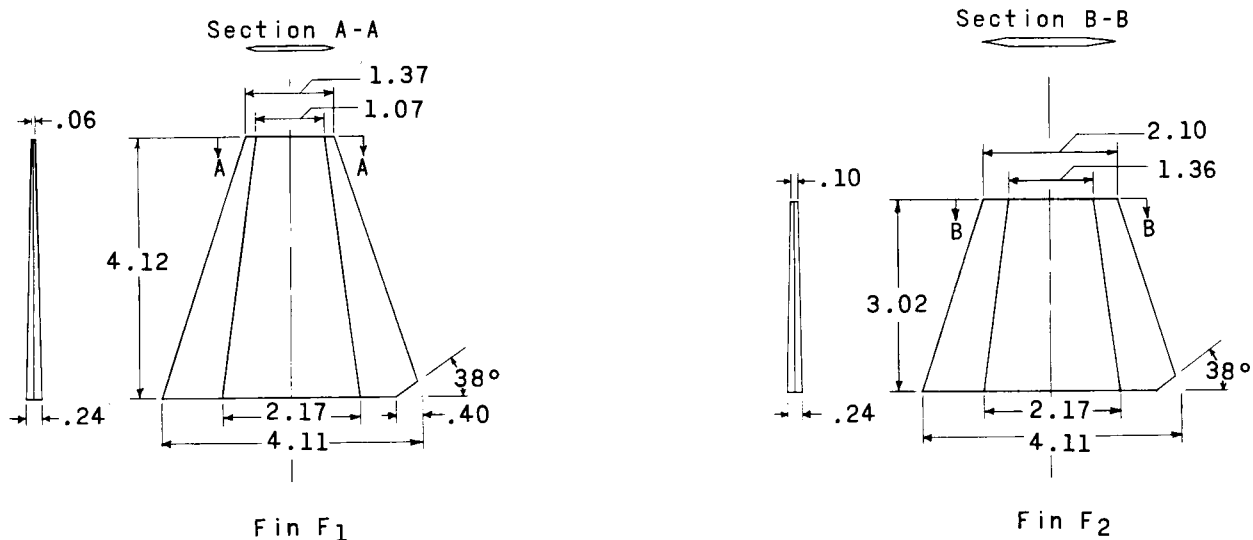


Figure 1.- Axes system. Arrows denote positive direction.

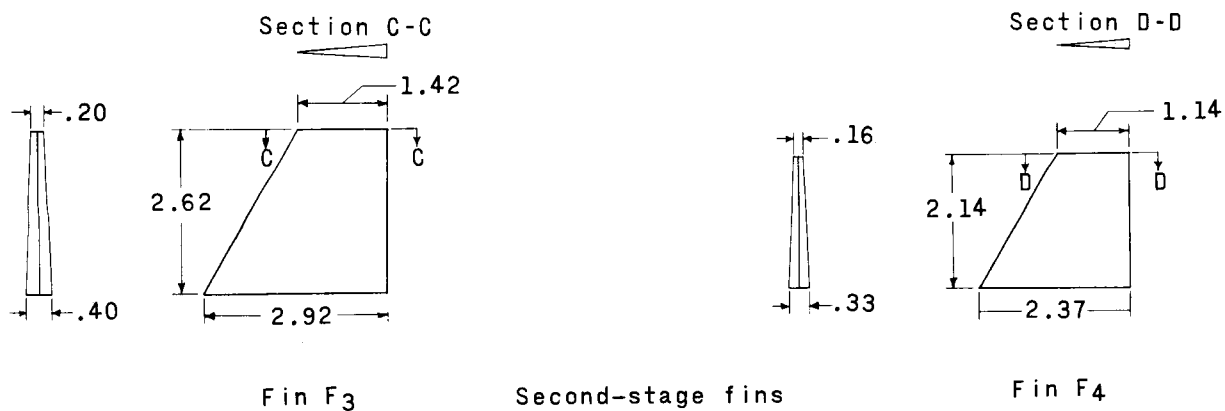


(a) Sketch of 1/12.4-scale models of two three-stage configurations.

Figure 2.- Dimensional details of models used in the investigation. All dimensions are in inches unless otherwise indicated.



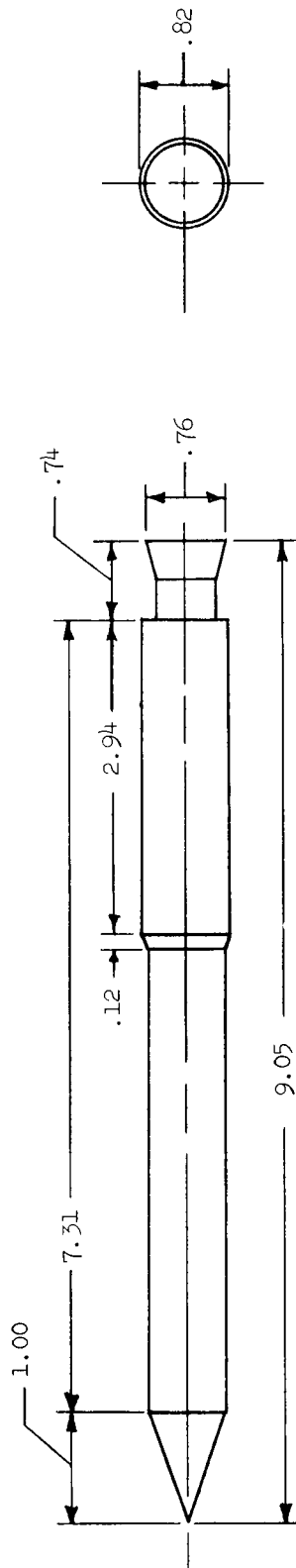
First-stage fins



Second-stage fins

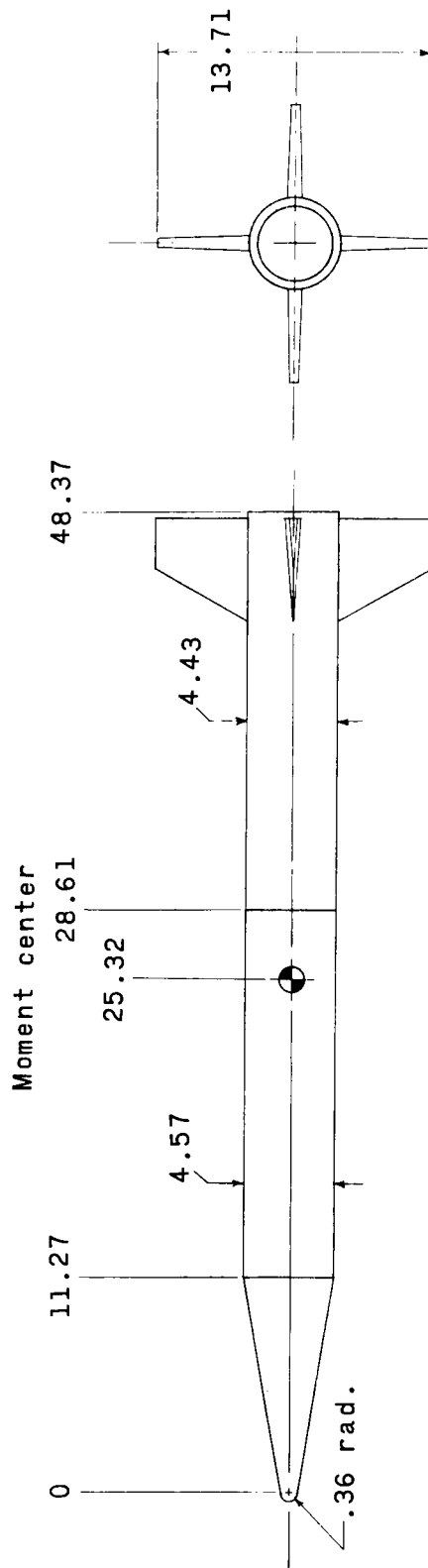
(b) 1/12.4-scale fins for three-stage models.

Figure 2.- Continued.



(c) First-stage auxiliary rocket motor.

Figure 2.- Continued.

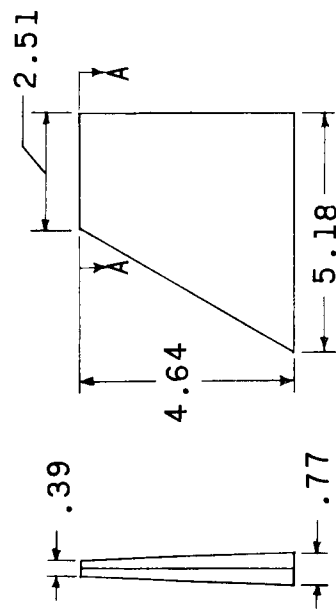


Model 3

(d) Sketch of 1/7-scale model of two-stage configuration.

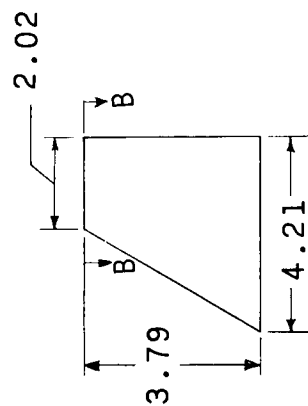
Figure 2.- Continued.

Section A-A



Fin F5

Section B-B

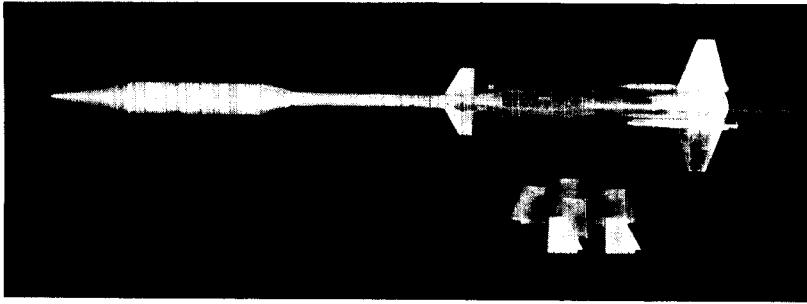


Fin F6

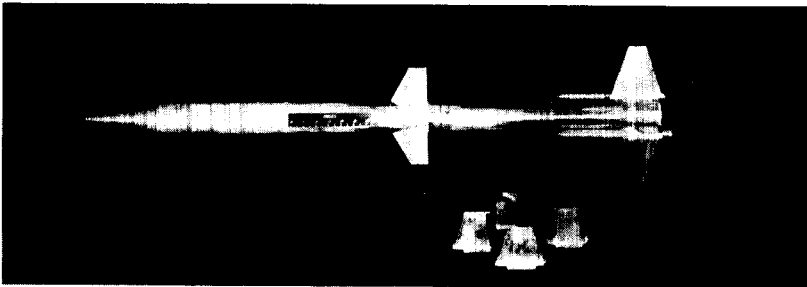
First-stage fins

(e) 1/7-scale fins for two-stage configuration.

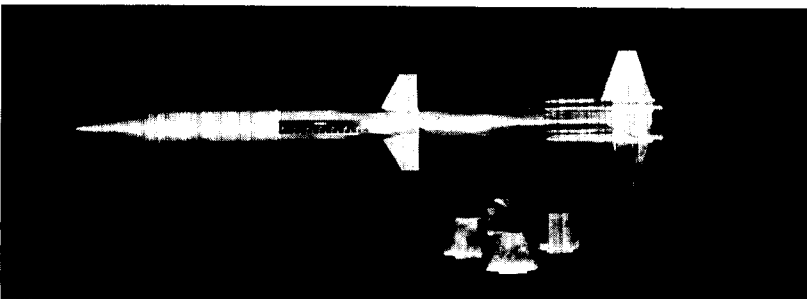
Figure 2.- Concluded.



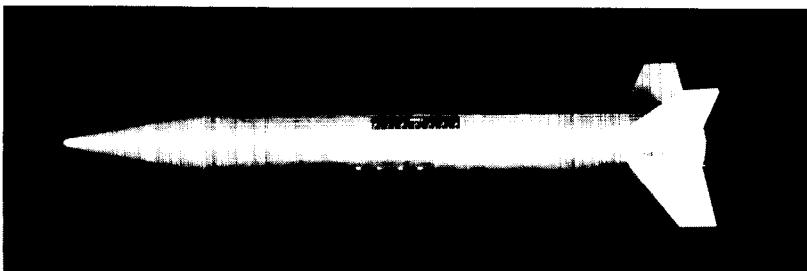
(a) Model 1.



(b) Model 2 with two auxiliary rocket motors.



(c) Model 2 with four auxiliary rocket motors.



(d) Model 3.

Figure 3.- Models used in the investigation. L-63-3118

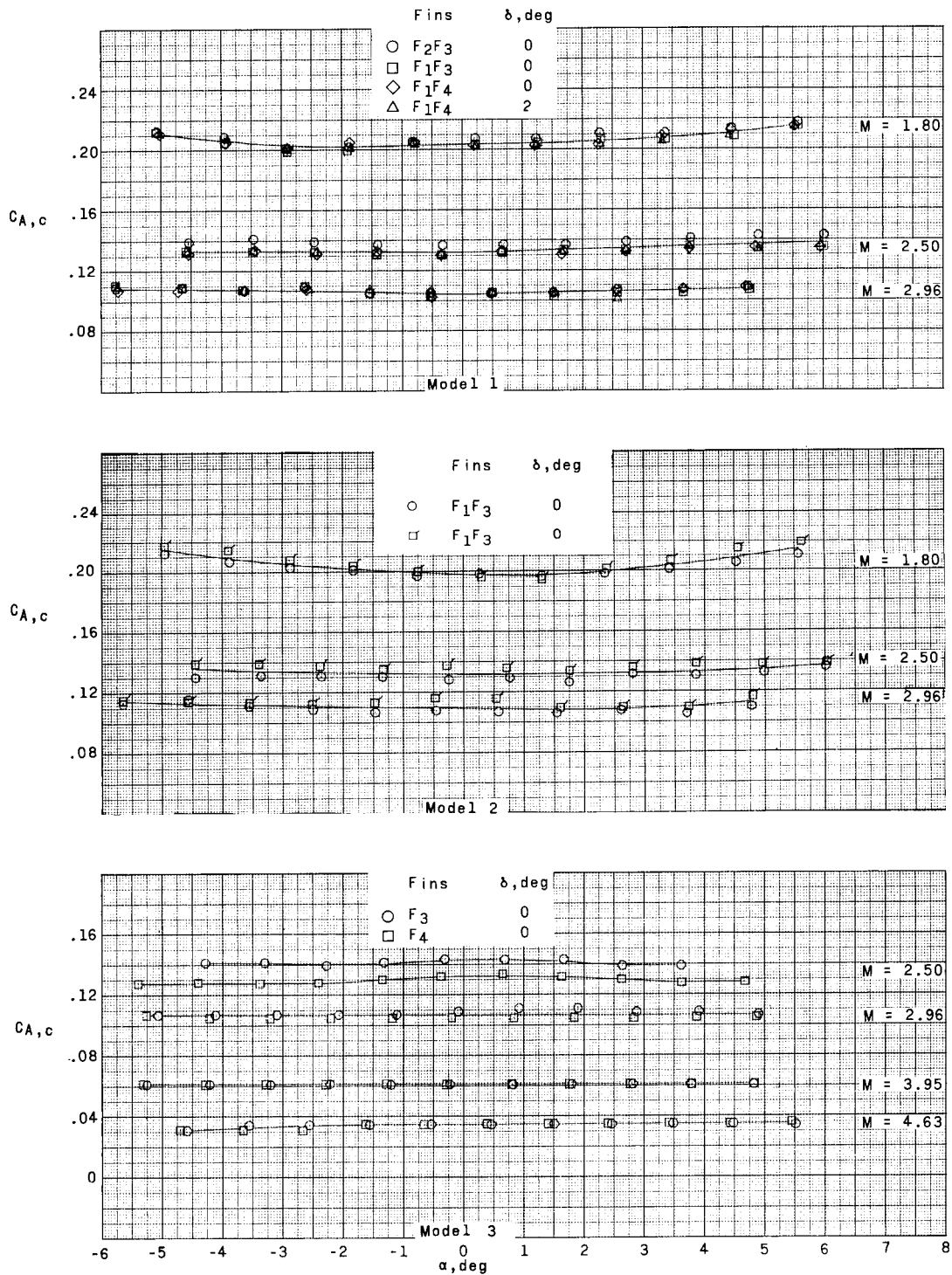
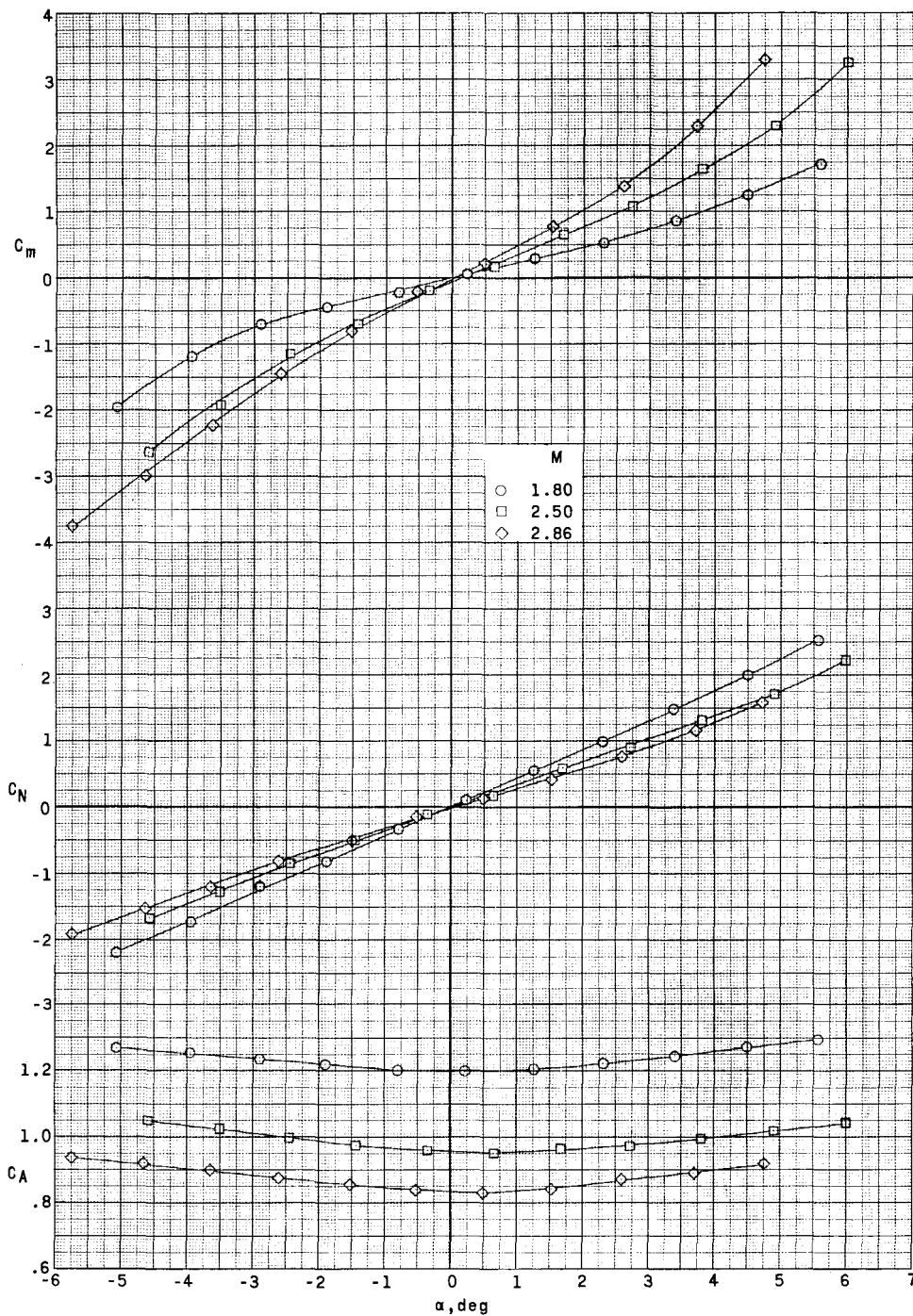
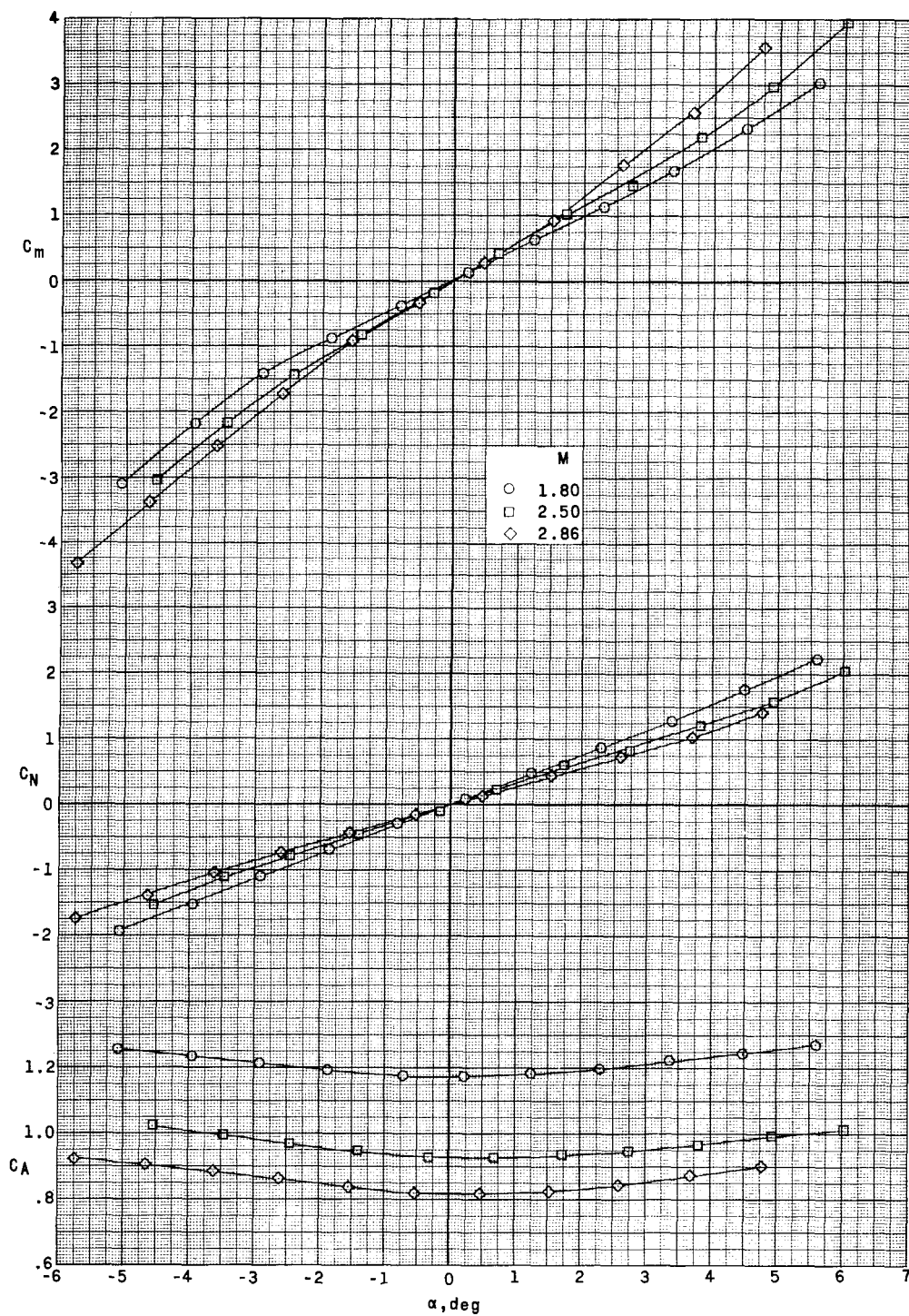


Figure 4.- Chamber axial-force coefficients for models 1, 2, and 3. (Plain symbols denote tests made with two auxiliary rocket motors; flagged symbols denote tests made with four auxiliary rocket motors.)



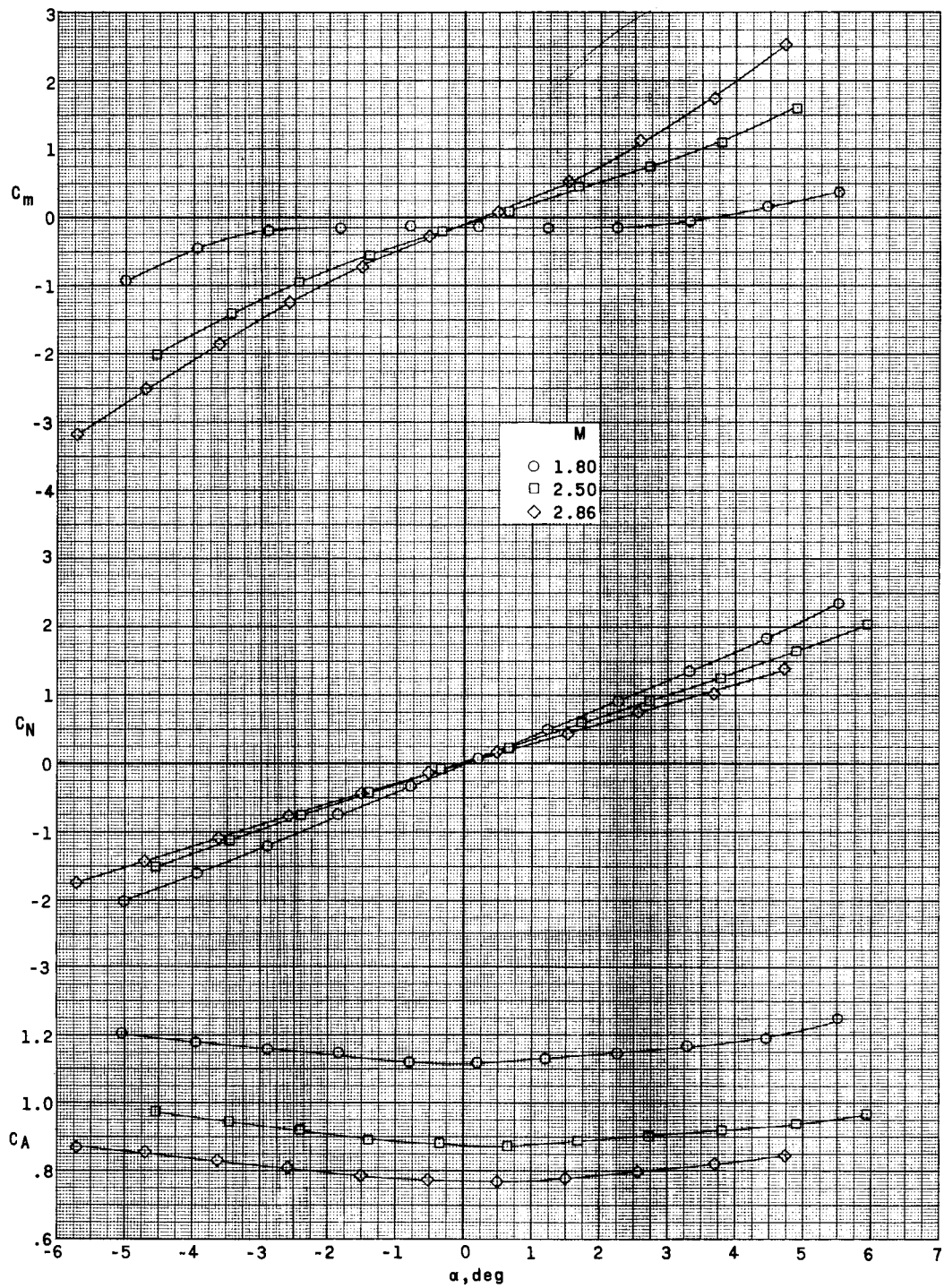
(a) Fins $F_1 F_3$; $\delta_I = \delta_{II} = 0^\circ$.

Figure 5.- Longitudinal aerodynamic characteristics of model 1 with two auxiliary rocket motors at several Mach numbers.



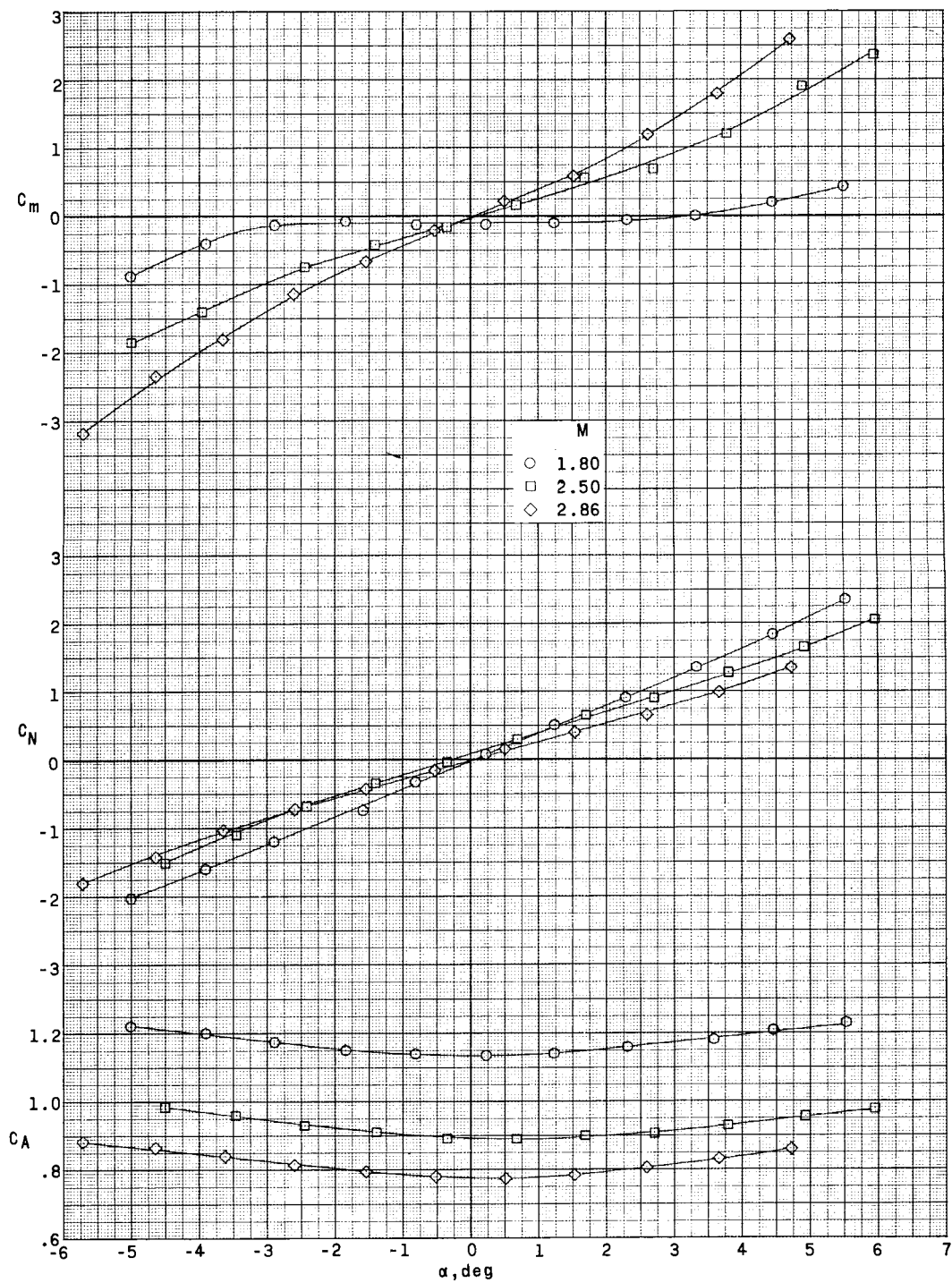
(b) Fins F_2F_3 ; $\delta_I = \delta_{II} = 0^\circ$.

Figure 5.- Continued.



(c) Fins $F_1 F_4$; $\delta_I = \delta_{II} = 0^\circ$.

Figure 5.- Continued.



(d) Fins F_1F_4 ; $\delta_I = \delta_{II} = 2^\circ$.

Figure 5.- Concluded.

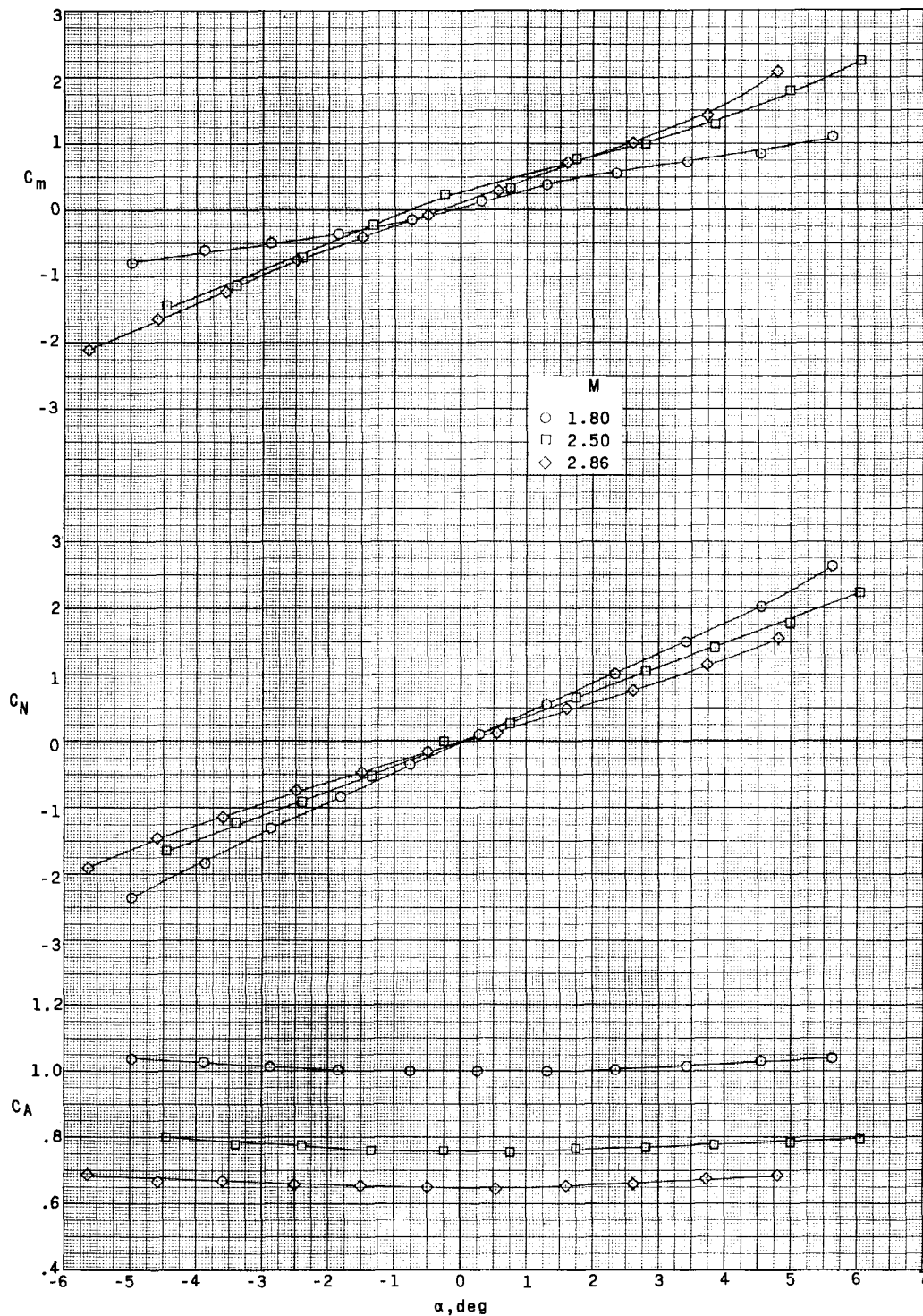


Figure 6.- Longitudinal aerodynamic characteristics of model 2 with two auxiliary rocket motors at several Mach numbers. Fins $F_1 F_3$; $\delta_I = \delta_{II} = 0^\circ$.

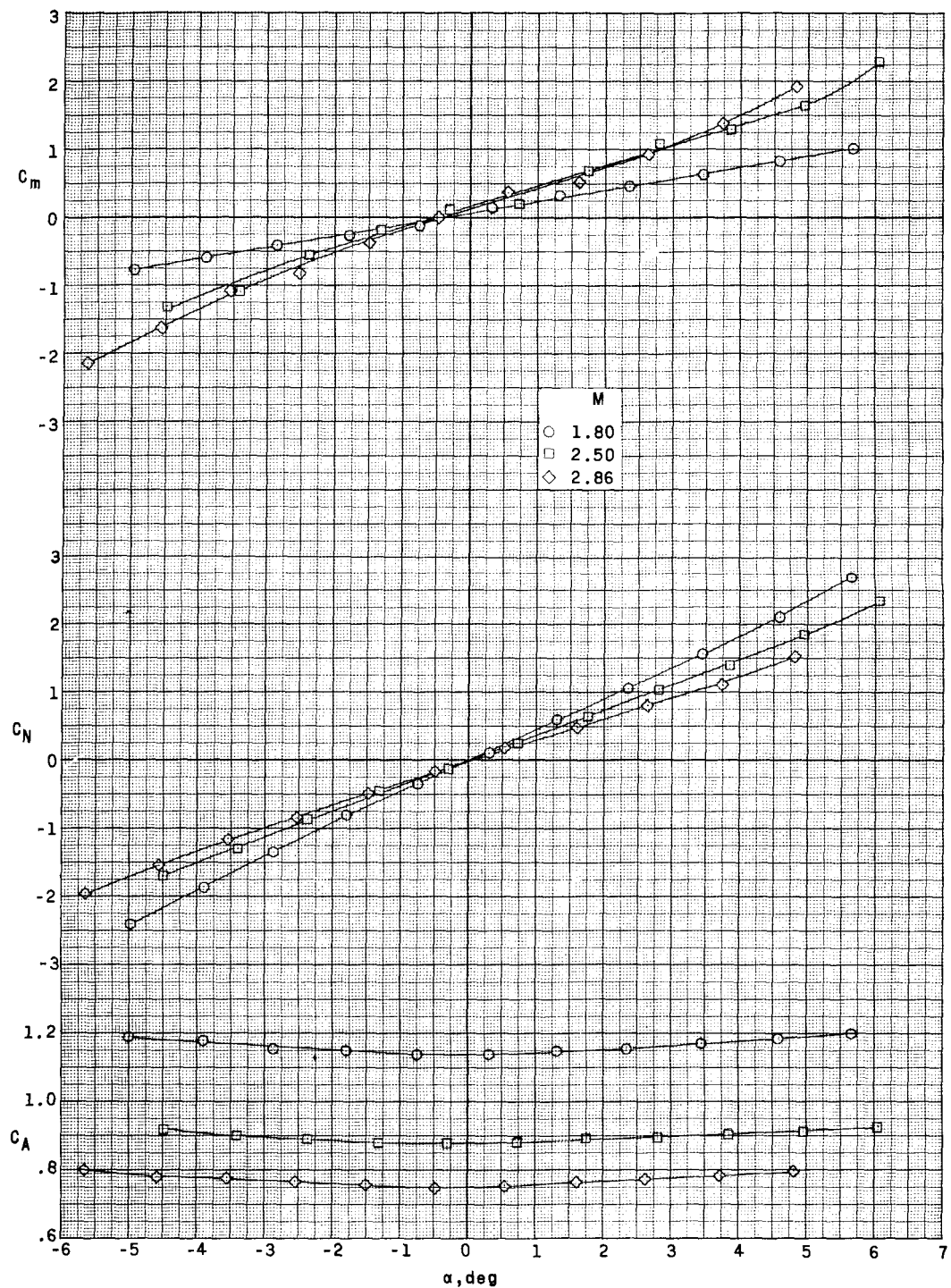
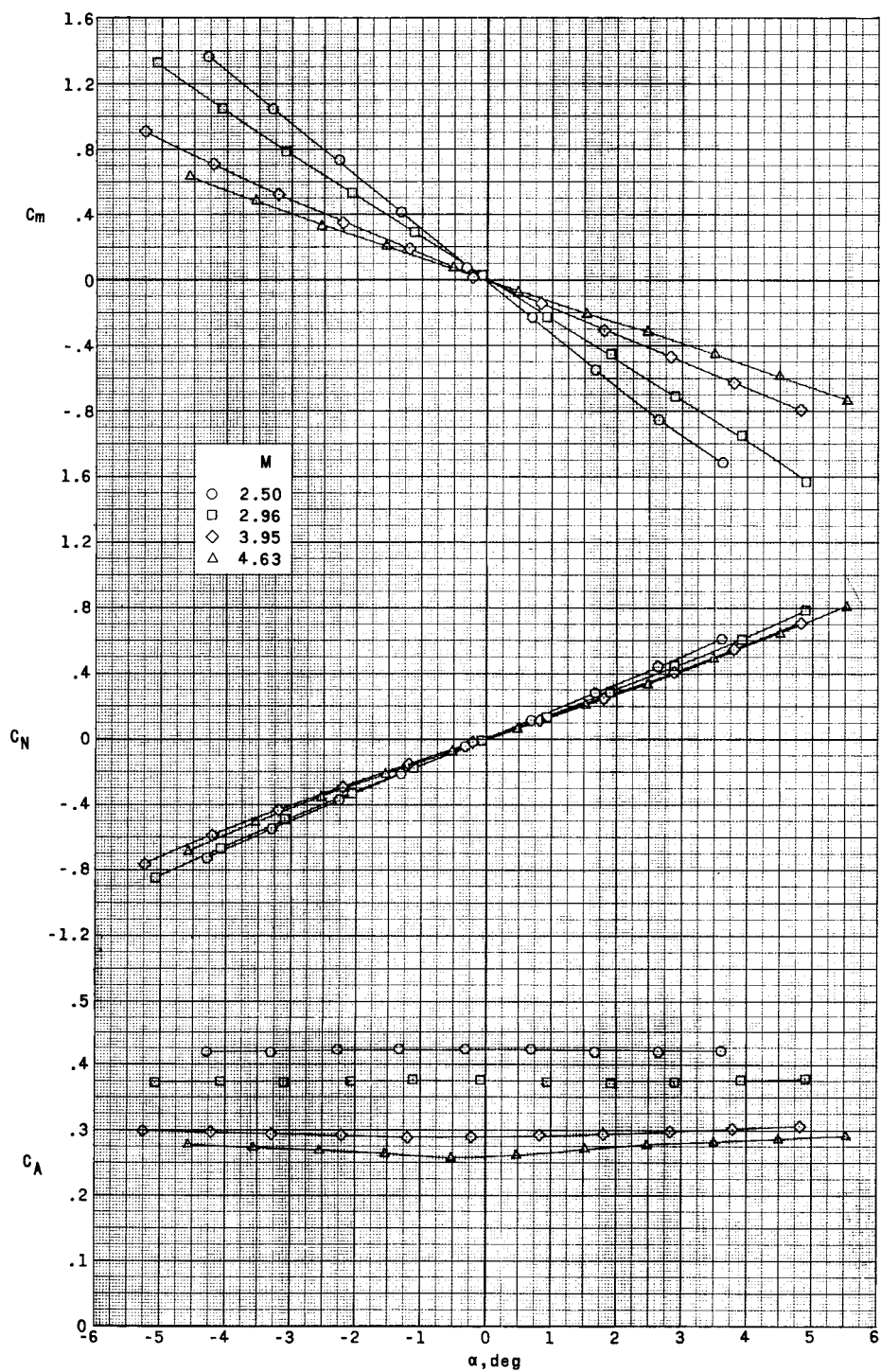
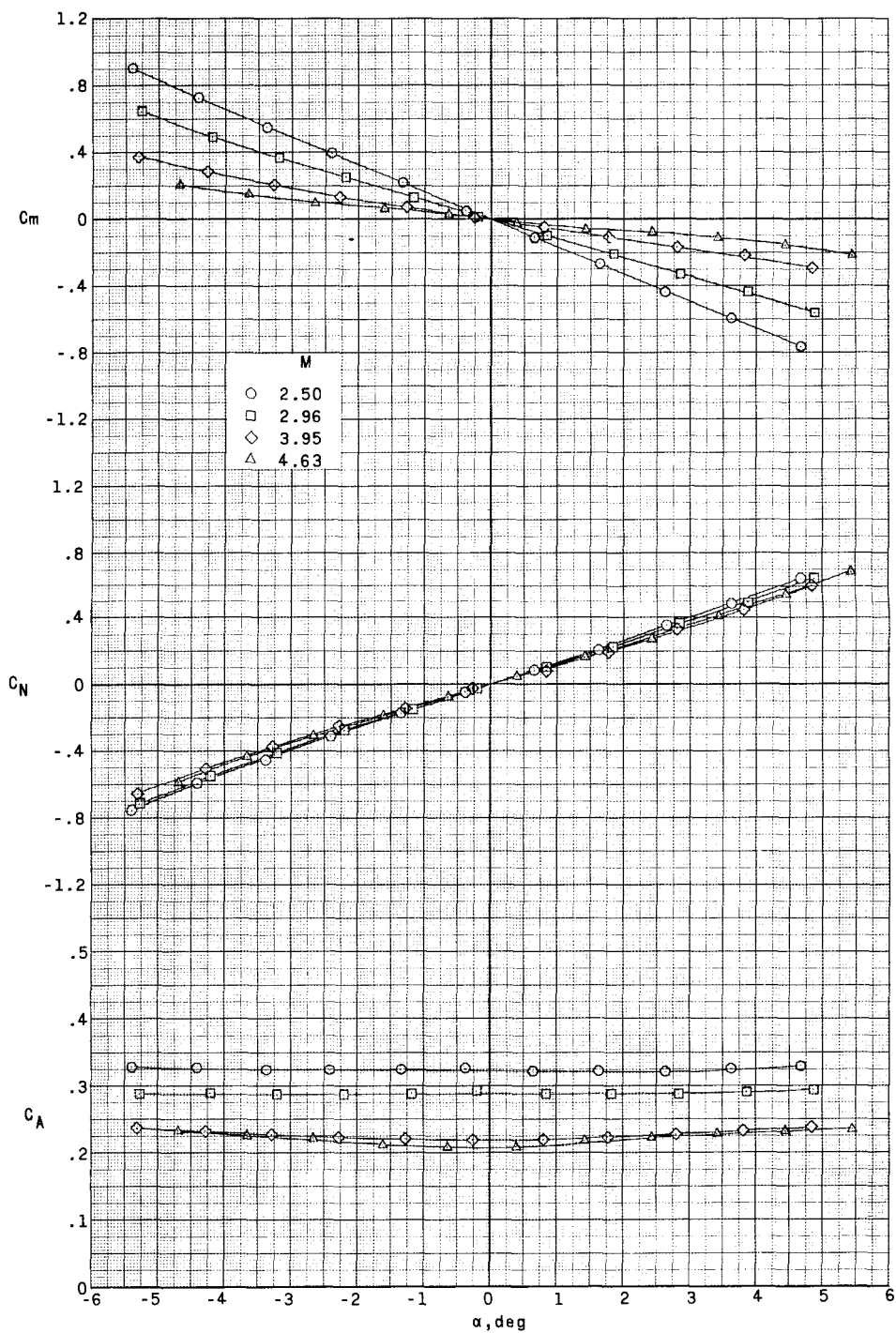


Figure 7.- Longitudinal aerodynamic characteristics of model 2 with four auxiliary rocket motors at several Mach numbers. Fins $F_1 F_3$; $\delta_I = \delta_{II} = 0^\circ$.



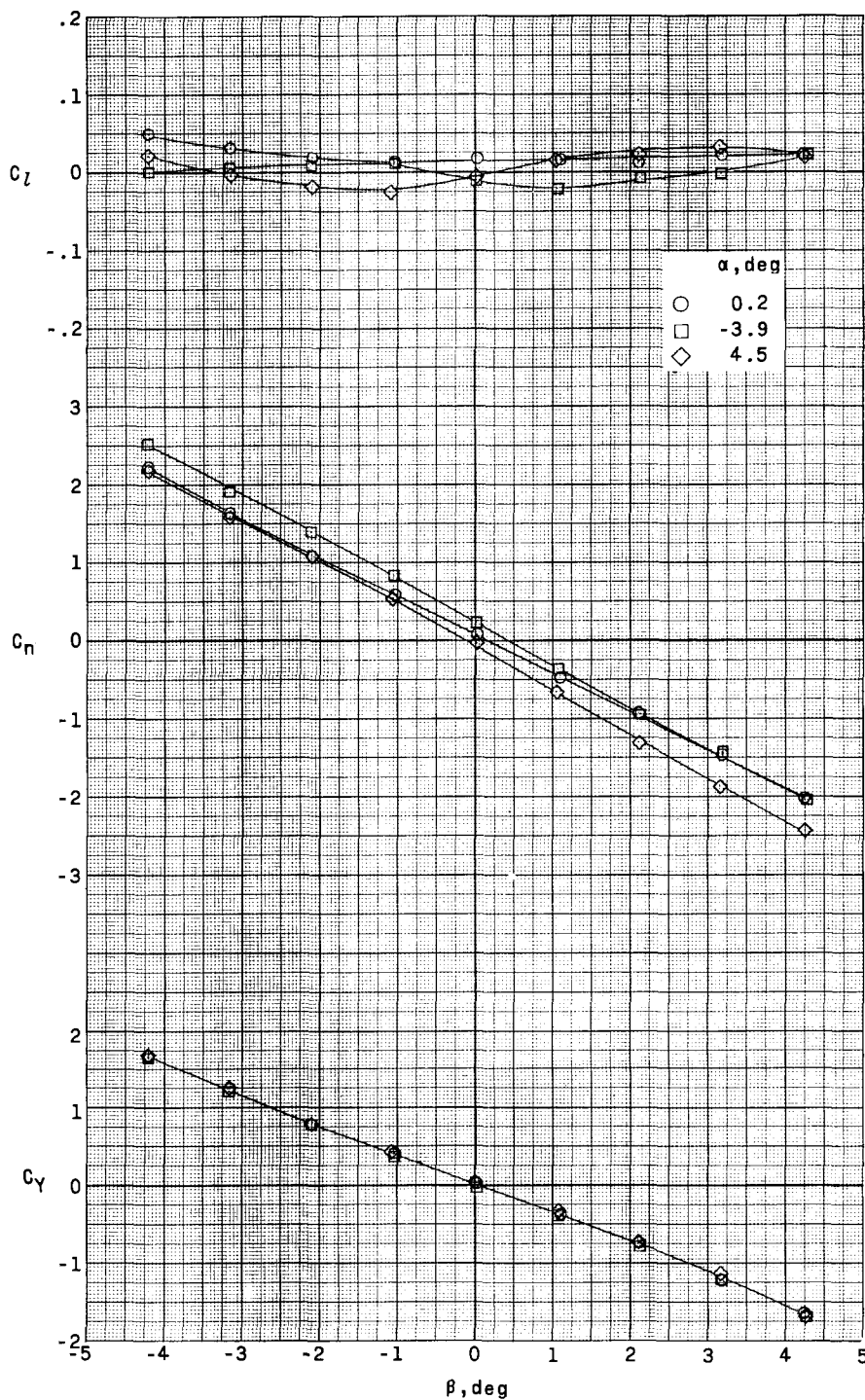
(a) Fin F_5 ; $\delta_I = 0^\circ$.

Figure 8.- Longitudinal aerodynamic characteristics of model 3 at several Mach numbers.



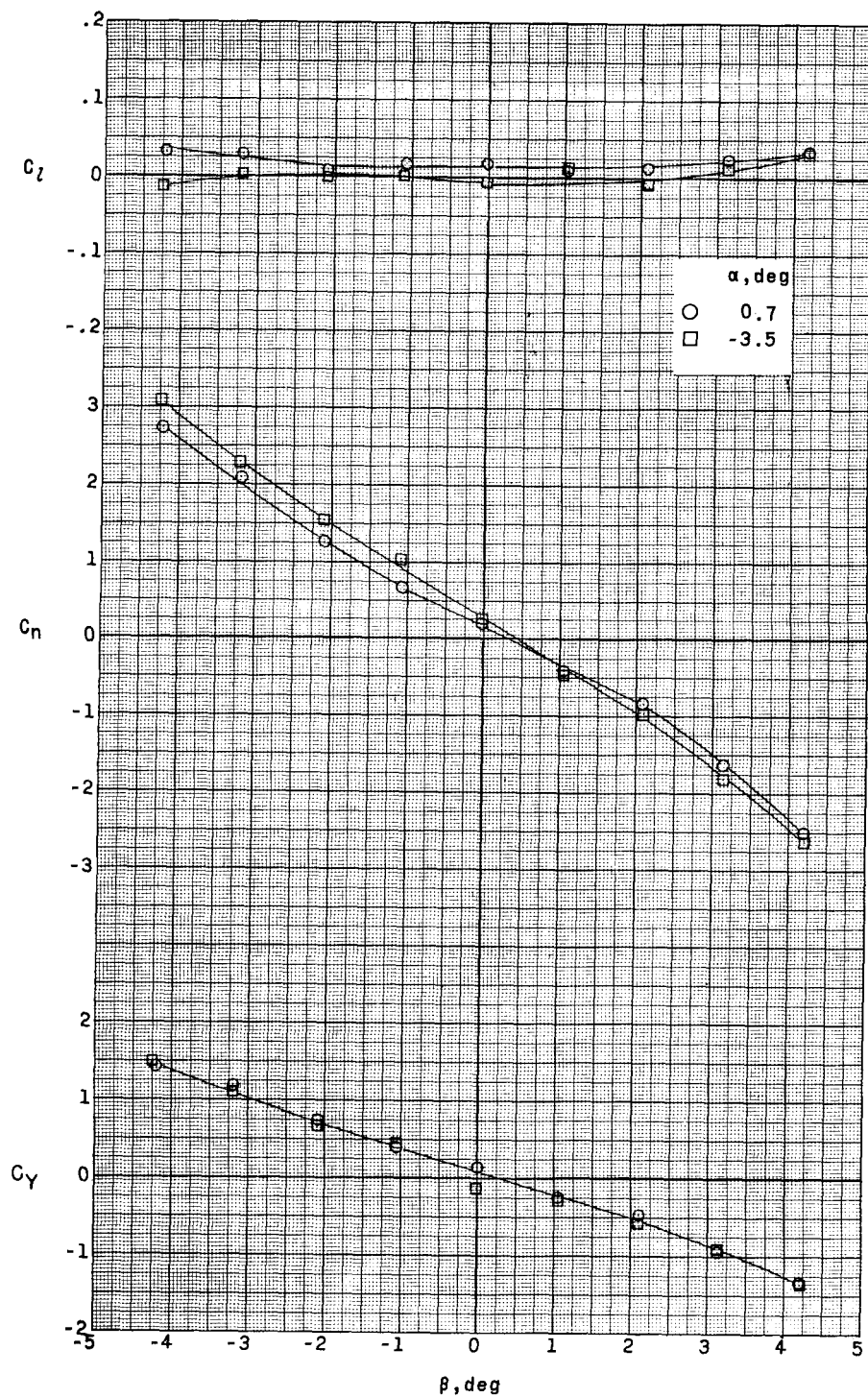
(b) Fin F_6 ; $\delta_I = 0^\circ$.

Figure 8.- Concluded.



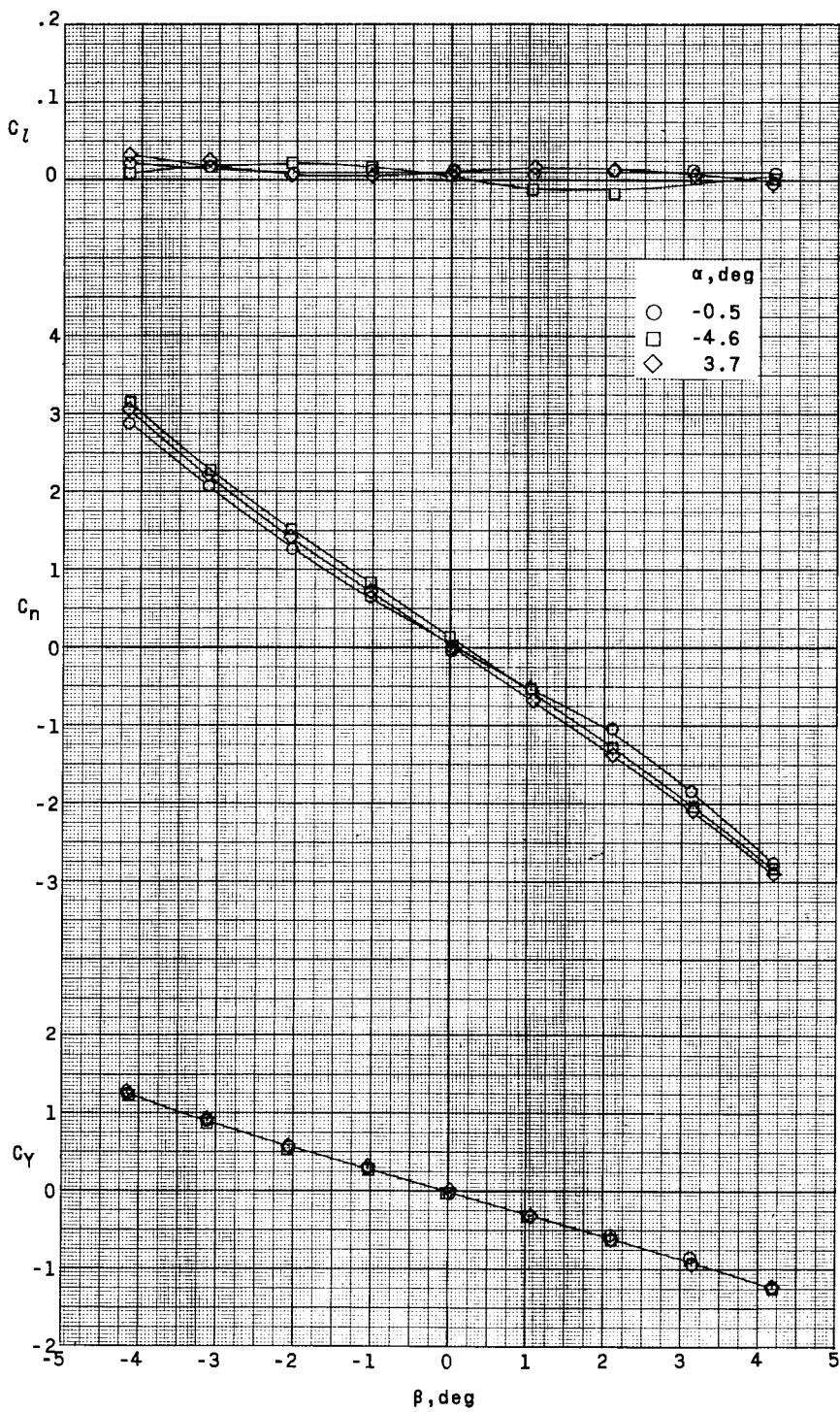
(a) $M = 1.80$; fins F_2F_3 ; $\delta_I = \delta_{II} = 0^\circ$.

Figure 9.- Lateral aerodynamic characteristics of model 1 with two auxiliary rocket motors at several angles of attack.



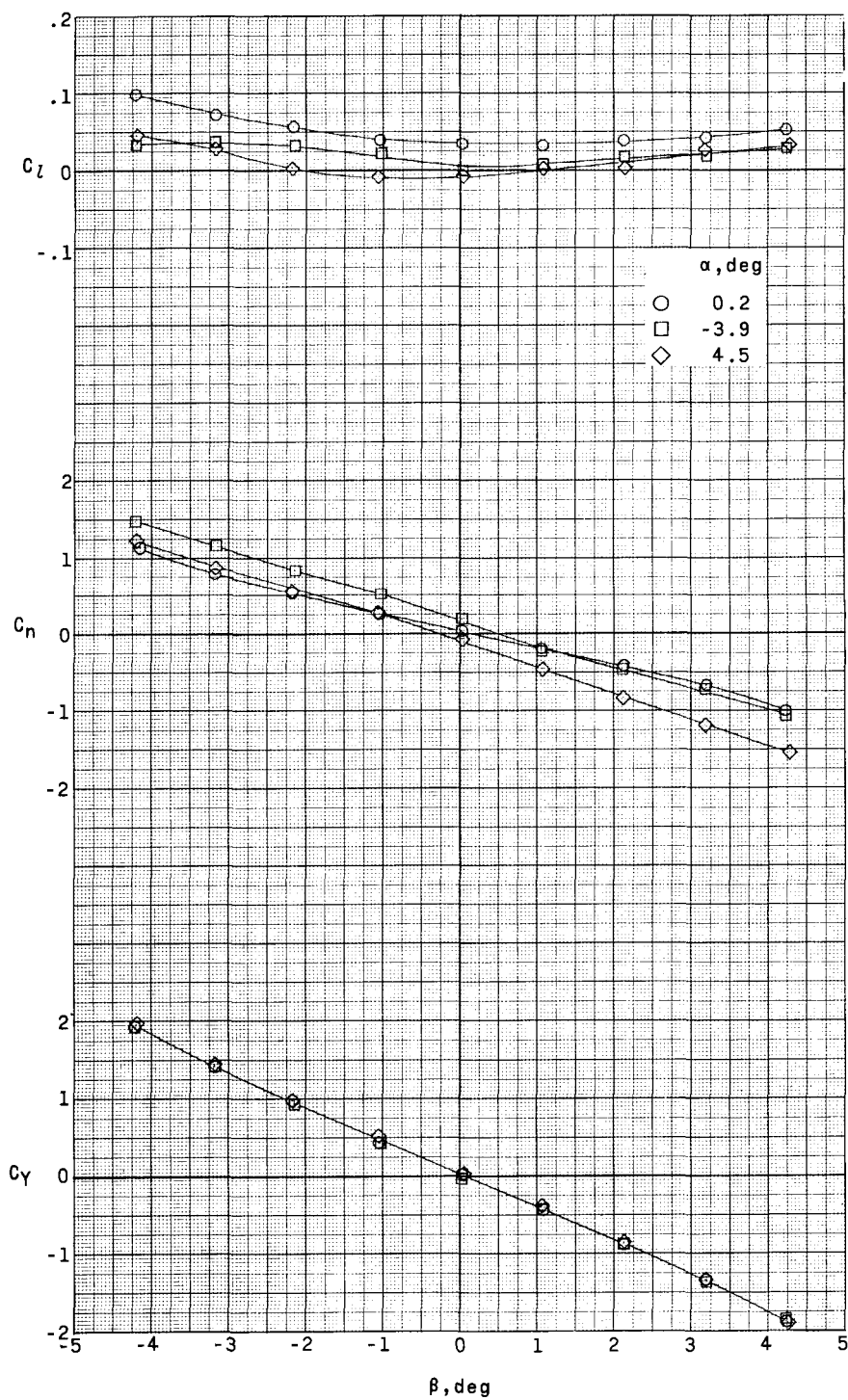
(b) $M = 2.50$; fins F_2F_3 ; $\delta_I = \delta_{II} = 0^\circ$.

Figure 9.- Continued.



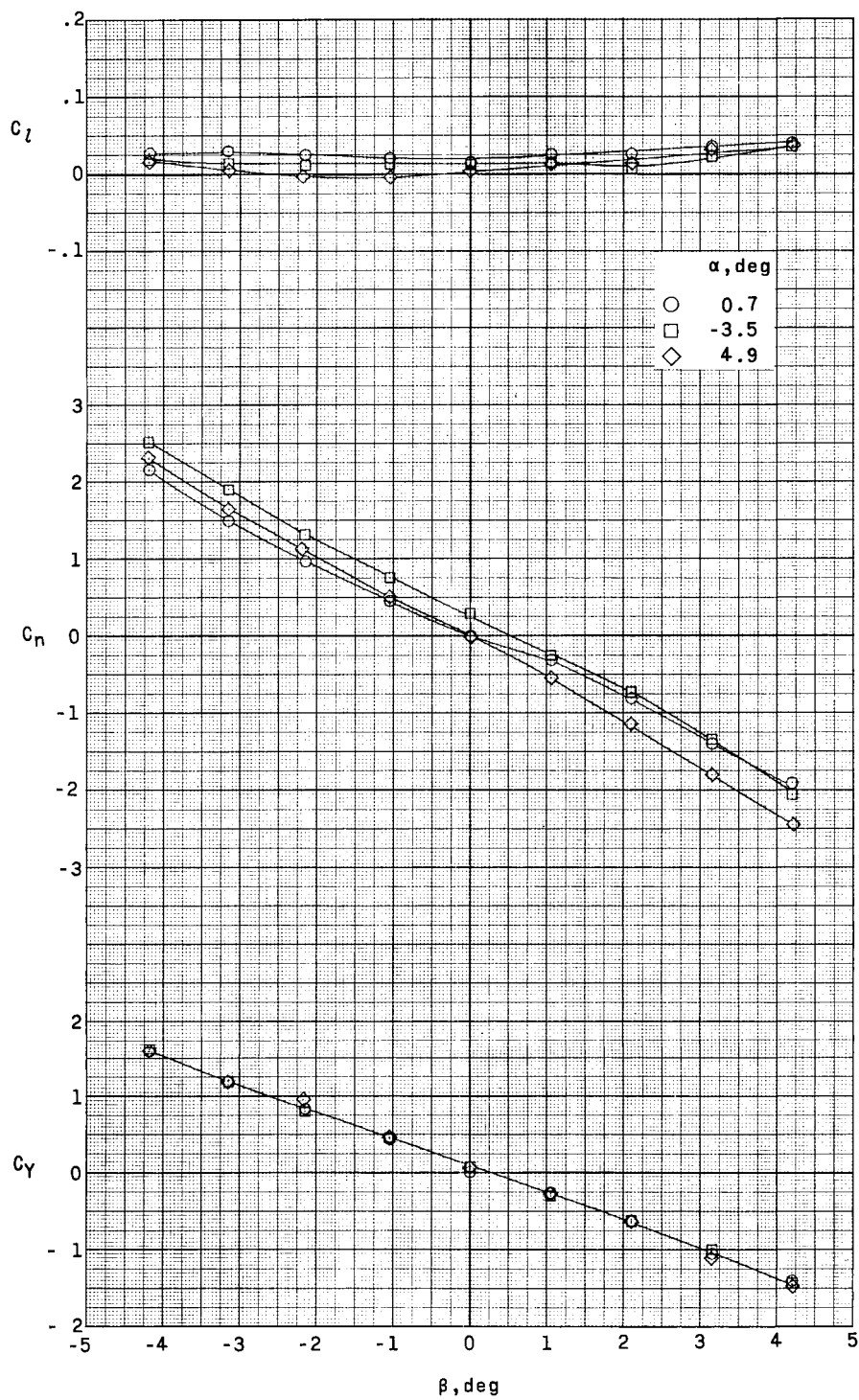
(c) $M = 2.86$; fins F_2F_3 ; $\delta_I = \delta_{II} = 0^\circ$.

Figure 9.- Continued.



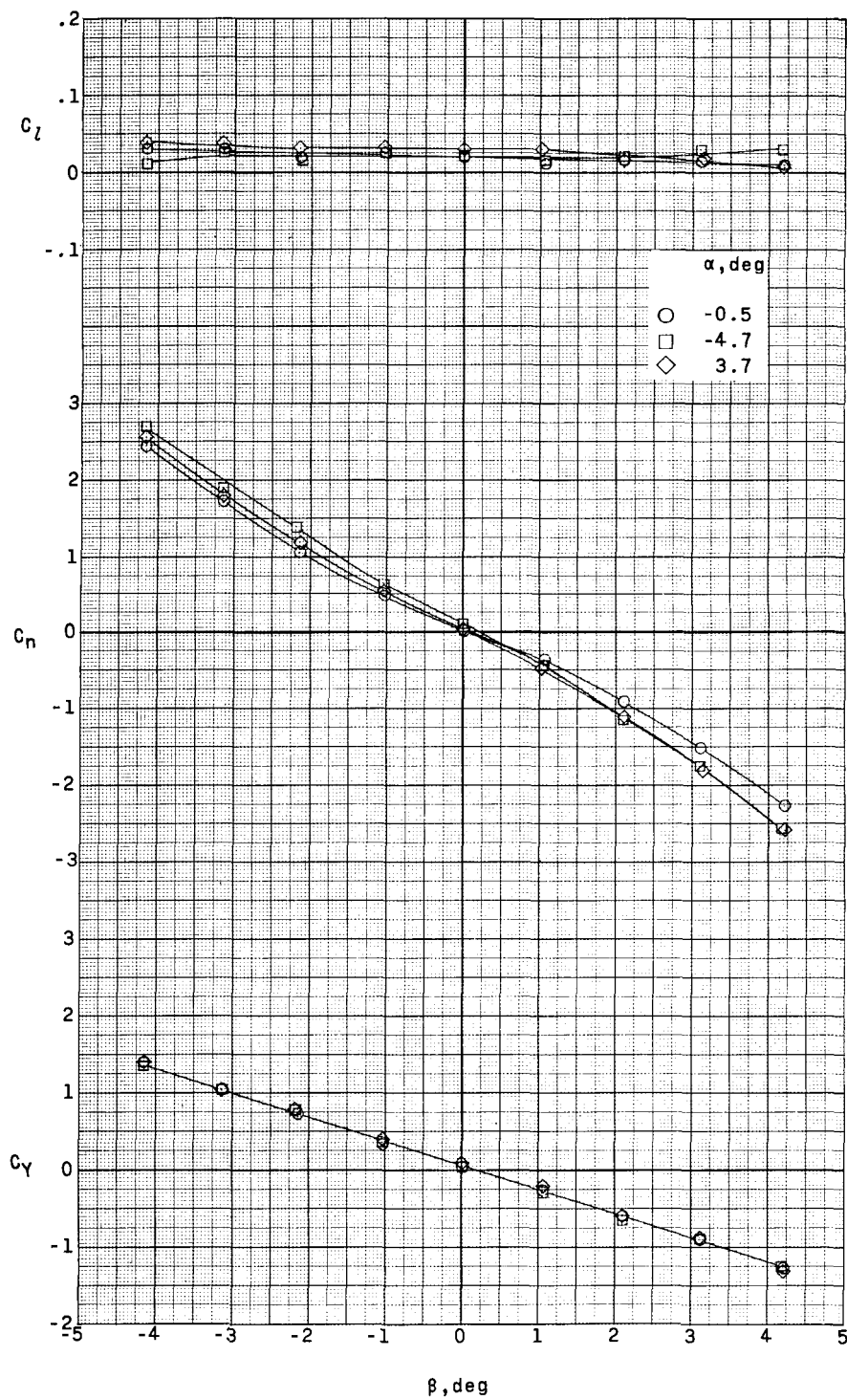
(d) $M = 1.80$; fins $F_1 F_3$; $\delta_I = \delta_{II} = 0^\circ$.

Figure 9.- Continued.



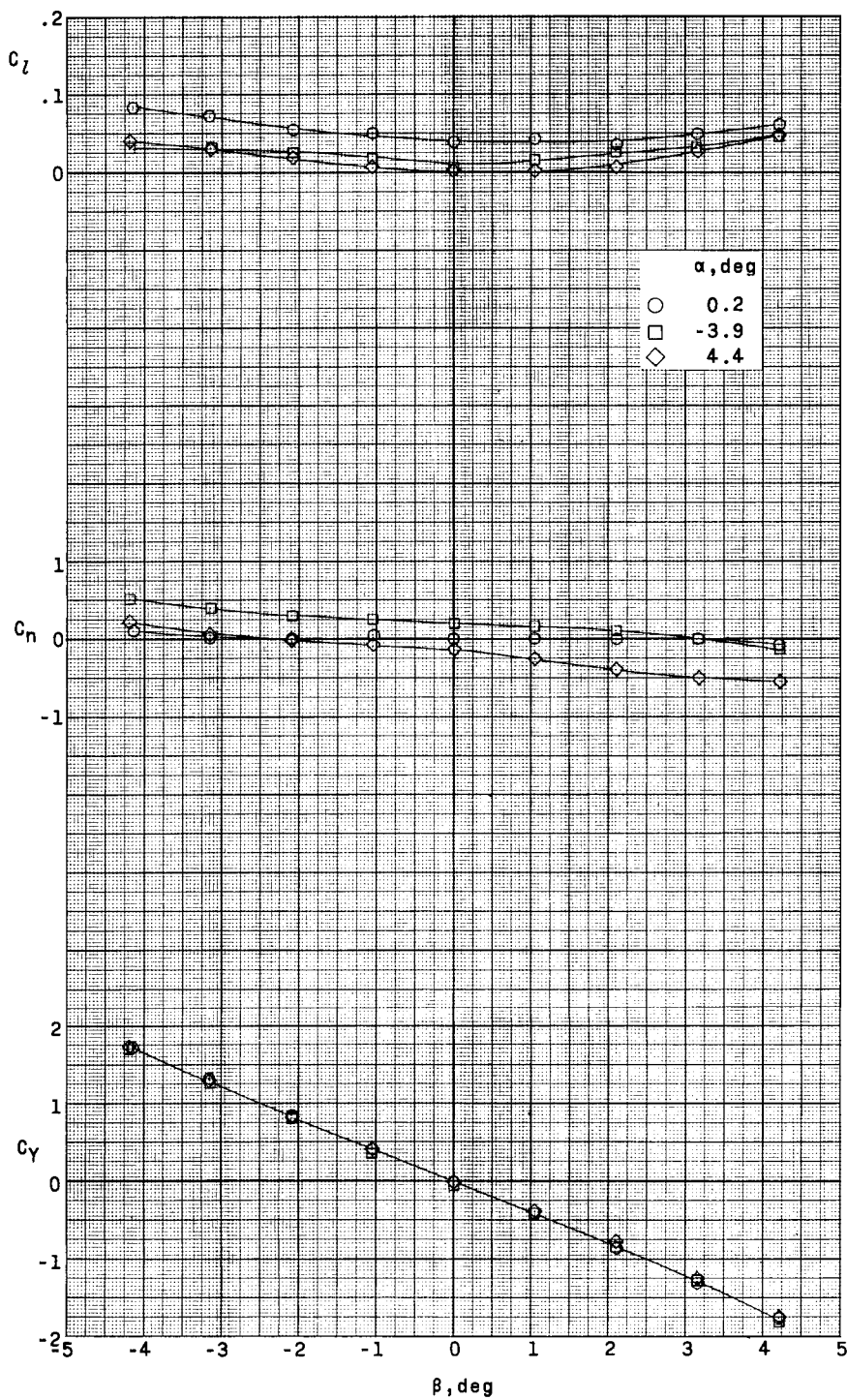
(e) $M = 2.50$; fins $F_1 F_3$; $\delta_I = \delta_{II} = 0^\circ$.

Figure 9.- Continued.



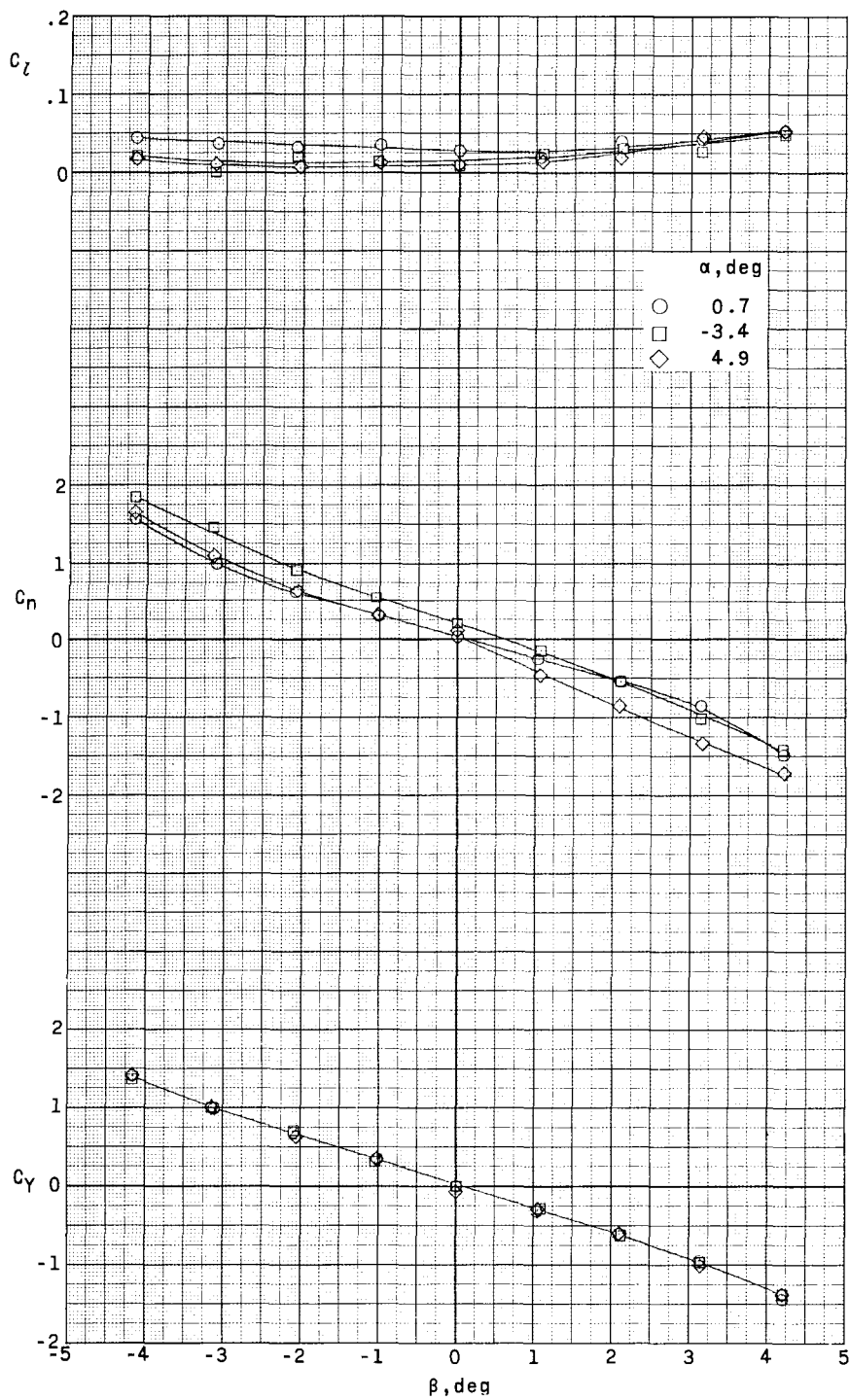
(f) $M = 2.86$; fins $F_1 F_3$; $\delta_I = \delta_{II} = 0^\circ$.

Figure 9.- Continued.



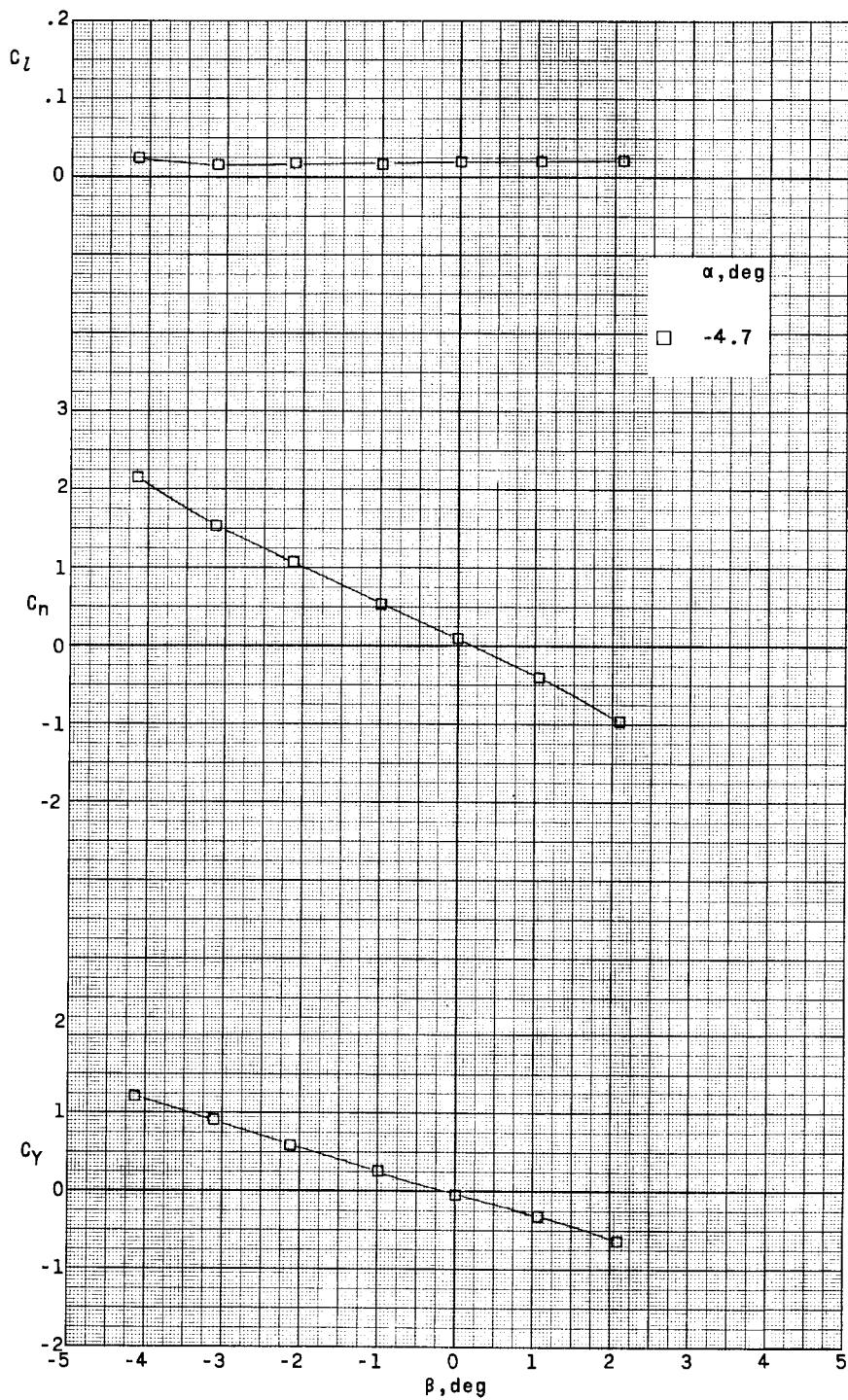
(g) $M = 1.80$; fins $F_1 F_4$; $\delta_I = \delta_{II} = 0^\circ$.

Figure 9.- Continued.



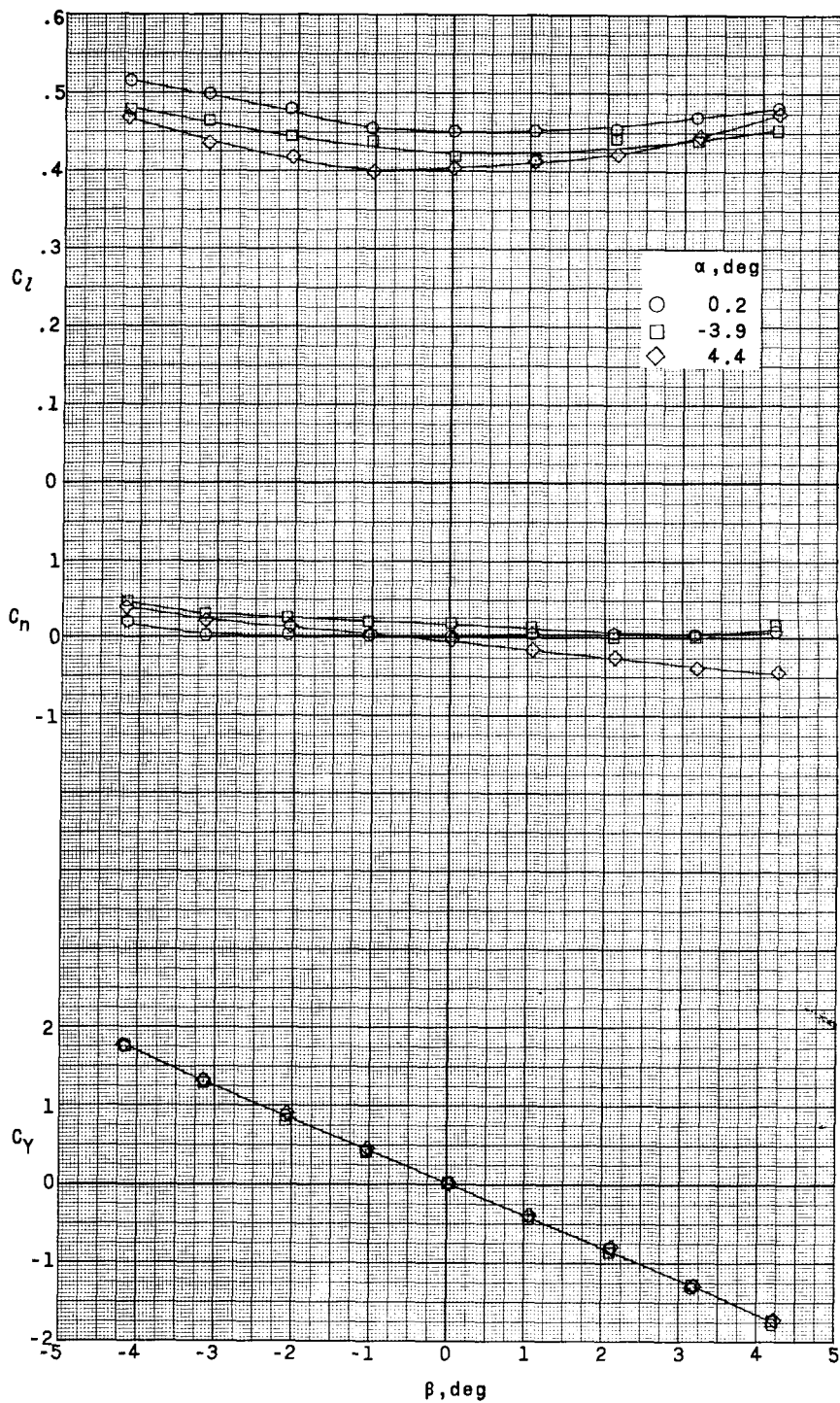
(h) $M = 2.50$; fins $F_1 F_4$; $\delta_I = \delta_{II} = 0^\circ$.

Figure 9.- Continued.



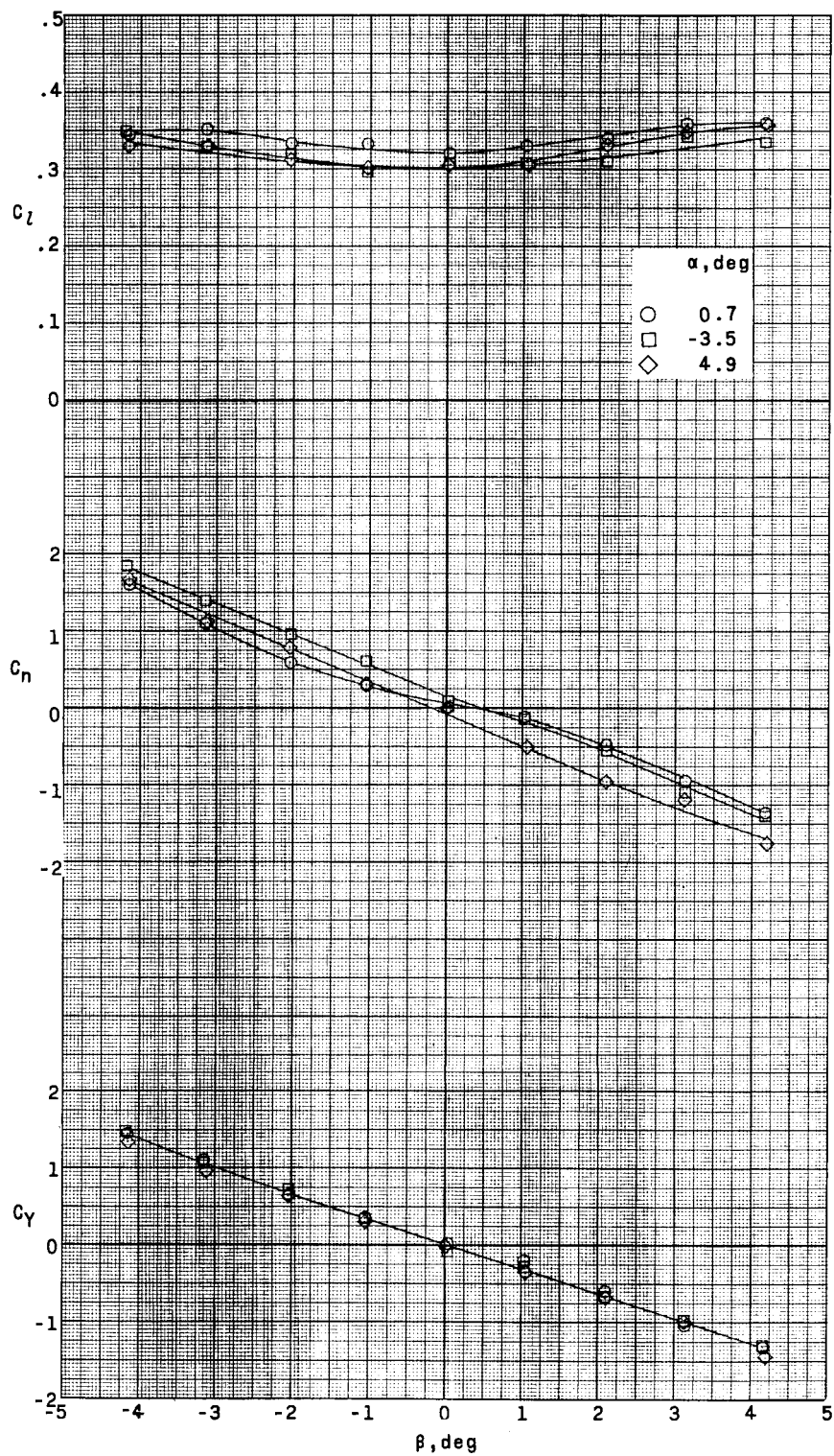
(i) $M = 2.86$; fins $F_1 F_4$; $\delta_I = \delta_{II} = 0^\circ$.

Figure 9.- Continued.



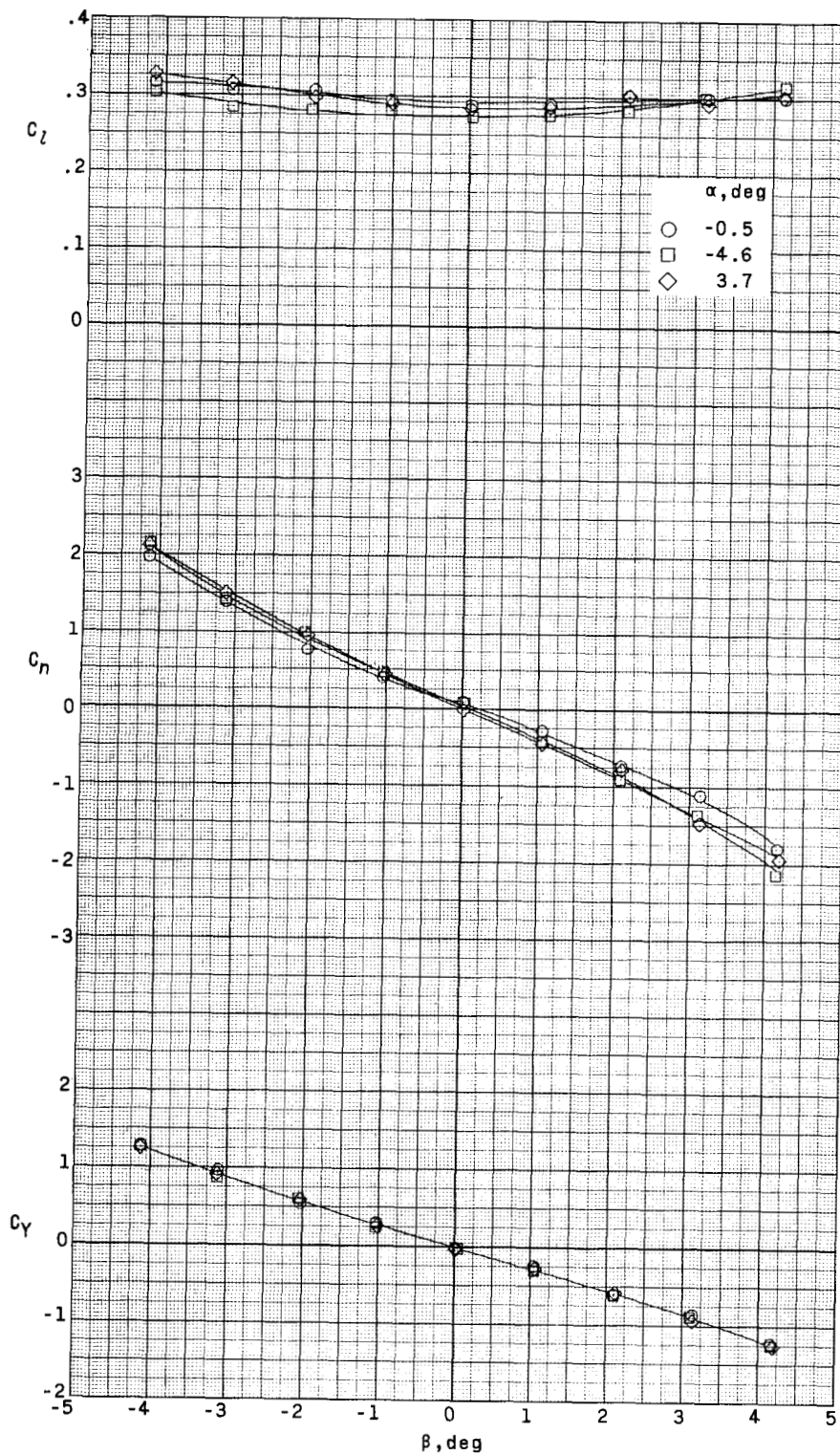
(j) $M = 1.80$; fins $F_1 F_4$; $\delta_I = \delta_{II} = 2^\circ$.

Figure 9.- Continued.



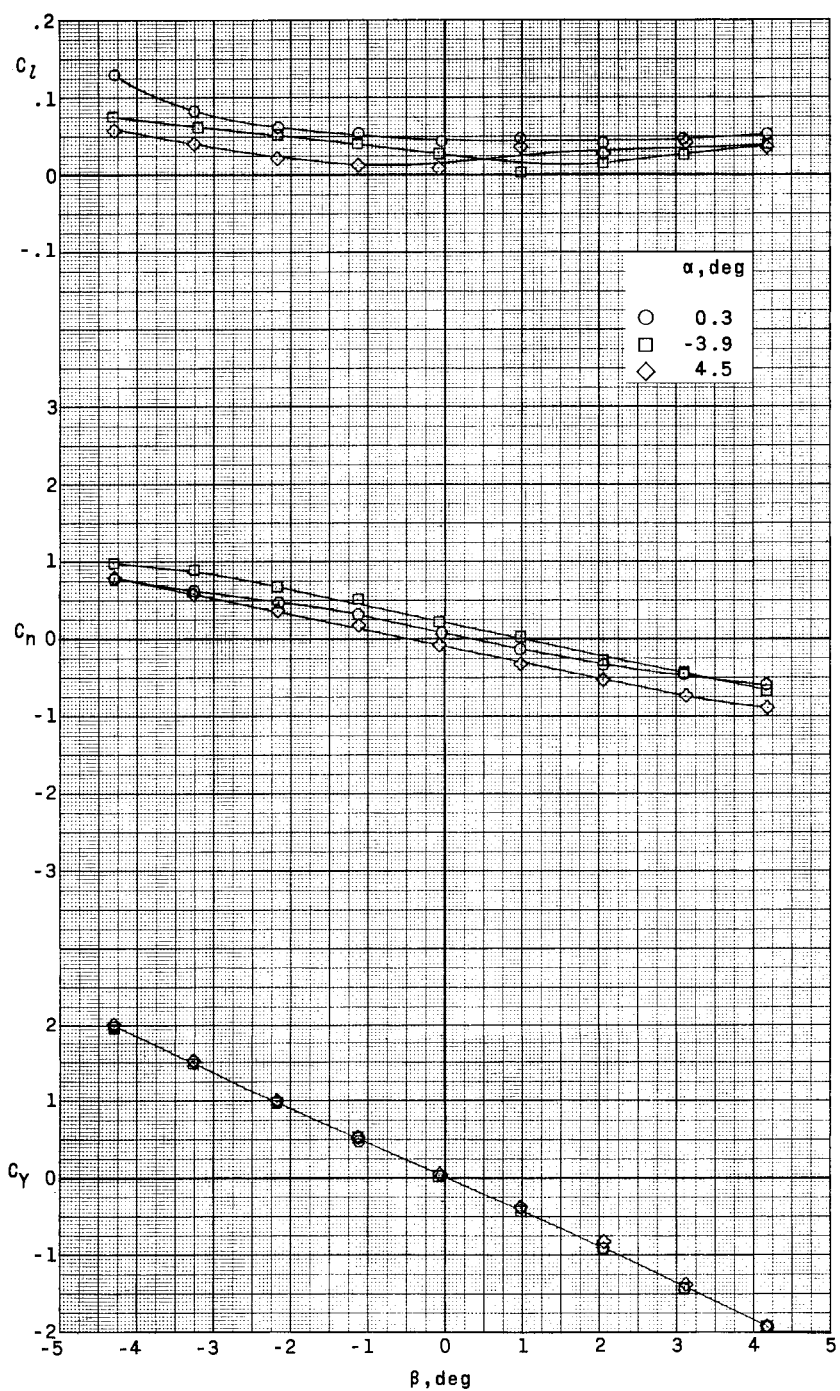
(k) $M = 2.50$; fins $F_1 F_4$; $\delta_I = \delta_{II} = 2^\circ$.

Figure 9.- Continued.



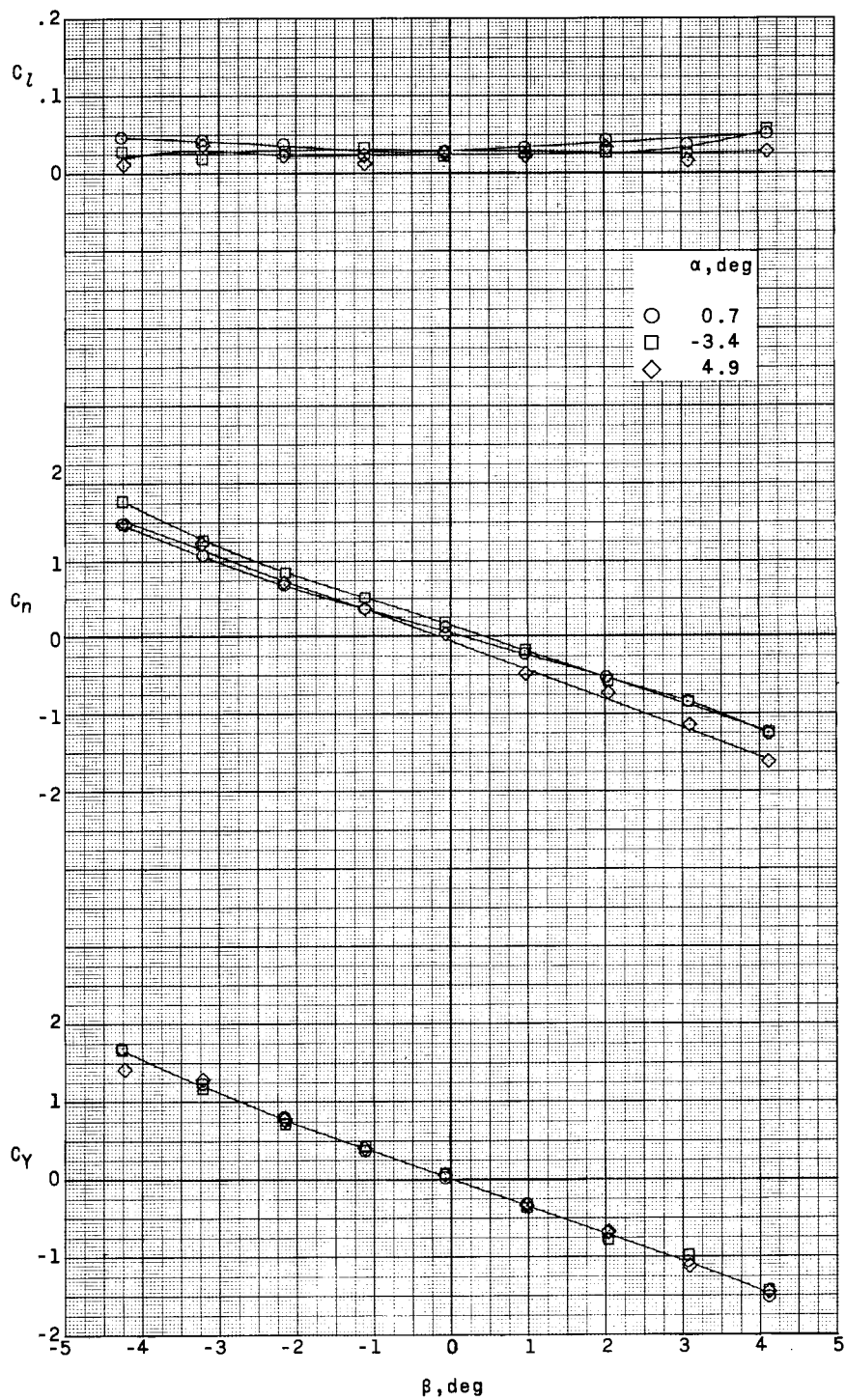
(2) $M = 2.86$; fins $F_1 F_4$; $\delta_I = \delta_{II} = 2^\circ$.

Figure 9.- Concluded.



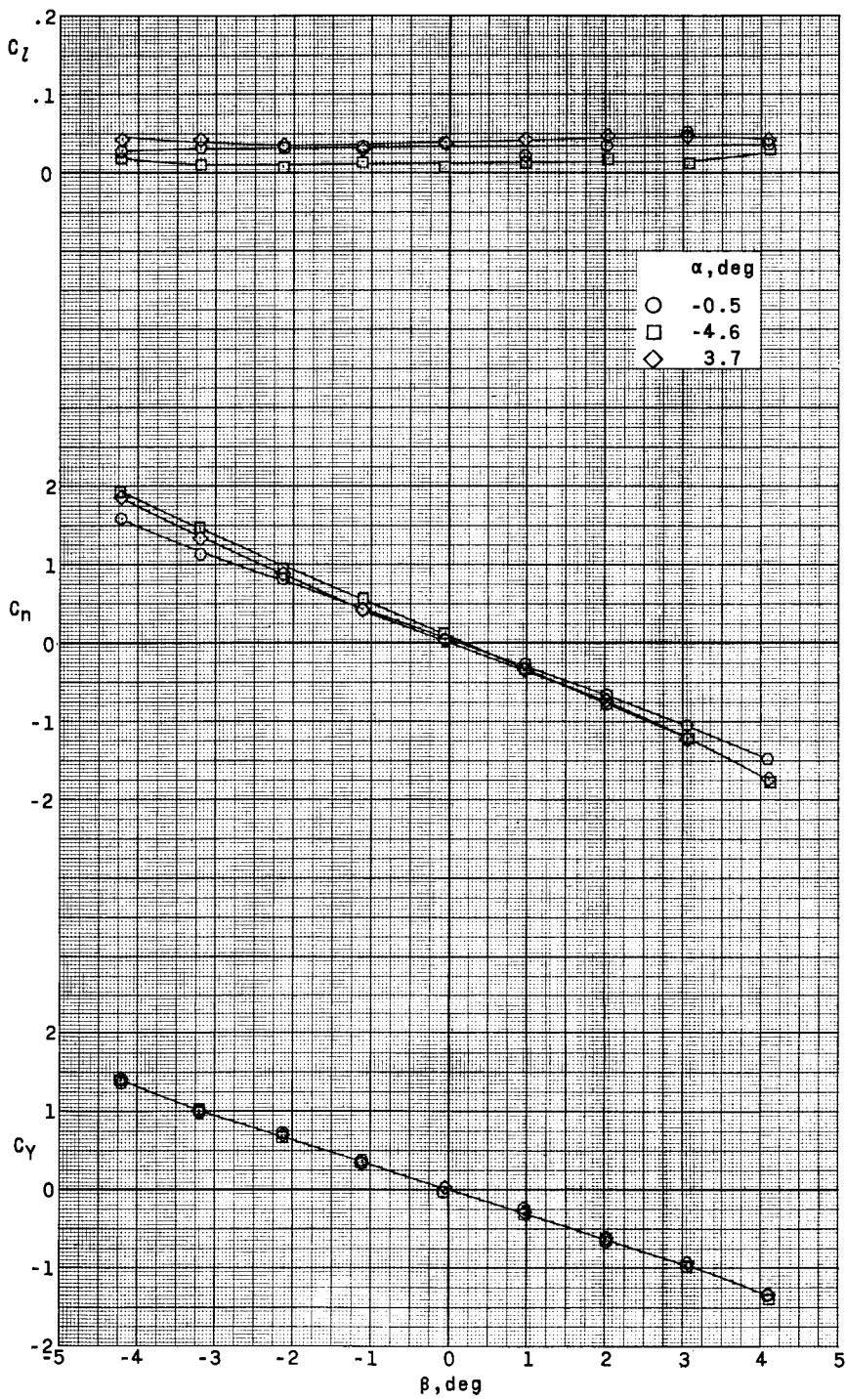
(a) $M = 1.80$; fins $F_1 F_3$; $\delta_I = \delta_{II} = 0^\circ$.

Figure 10.- Lateral aerodynamic characteristics of model 2 with two auxiliary rocket motors at several angles of attack.



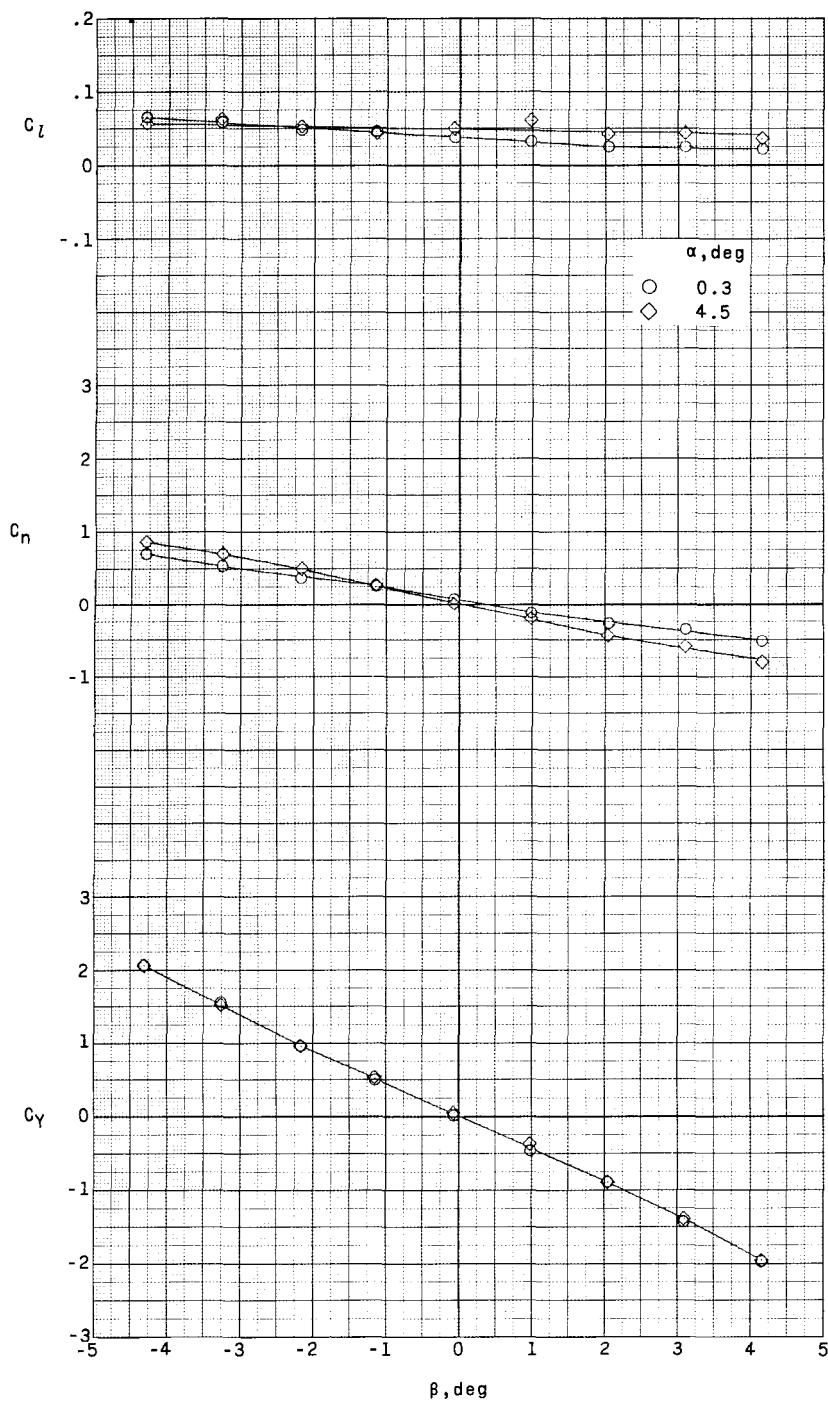
(b) $M = 2.50$; fins $F_1 F_3$; $\delta_I = \delta_{II} = 0^\circ$.

Figure 10.- Continued.



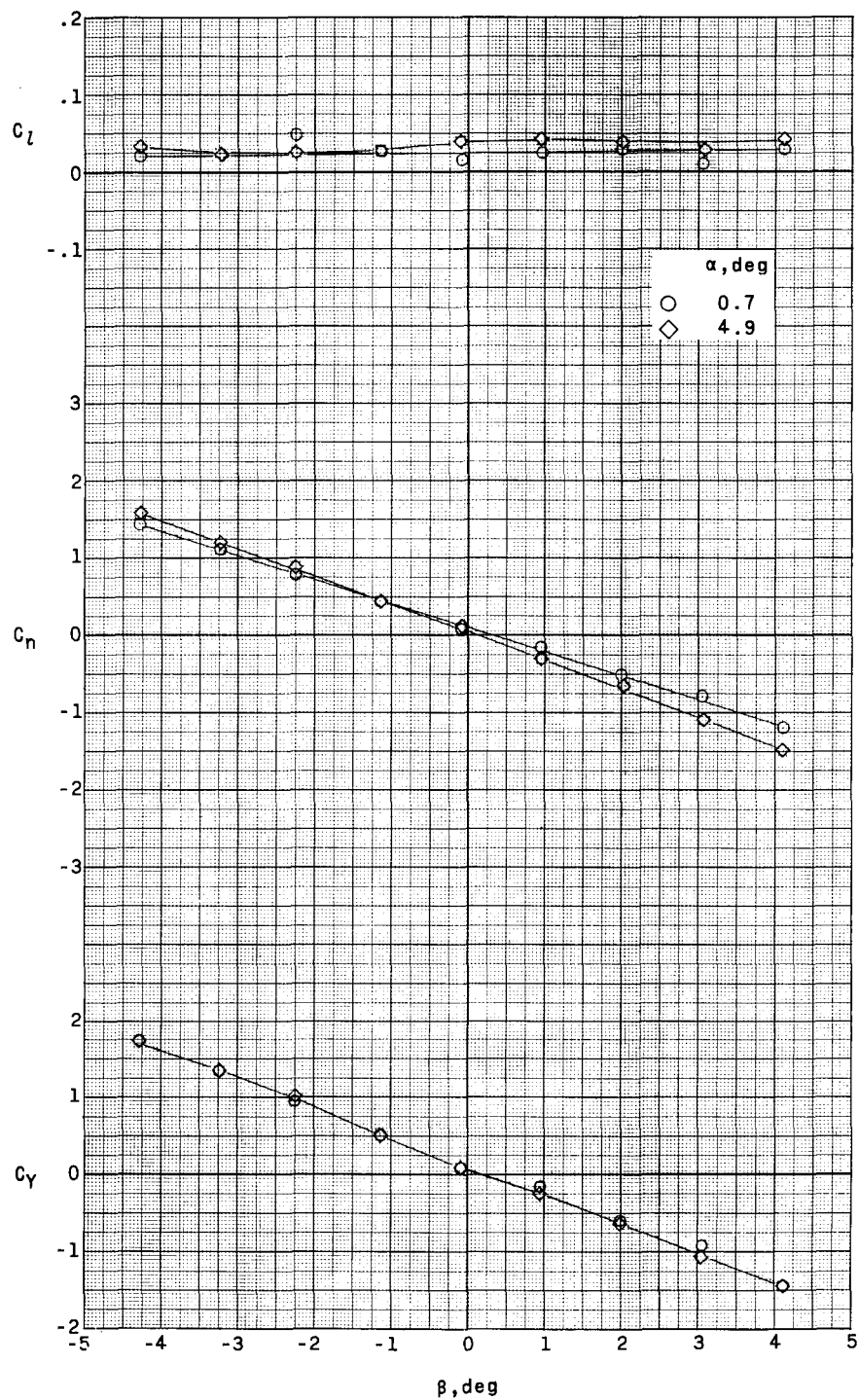
(c) $M = 2.86$; fins $F_1 F_3$; $\delta_I = \delta_{II} = 0^\circ$.

Figure 10.- Concluded.



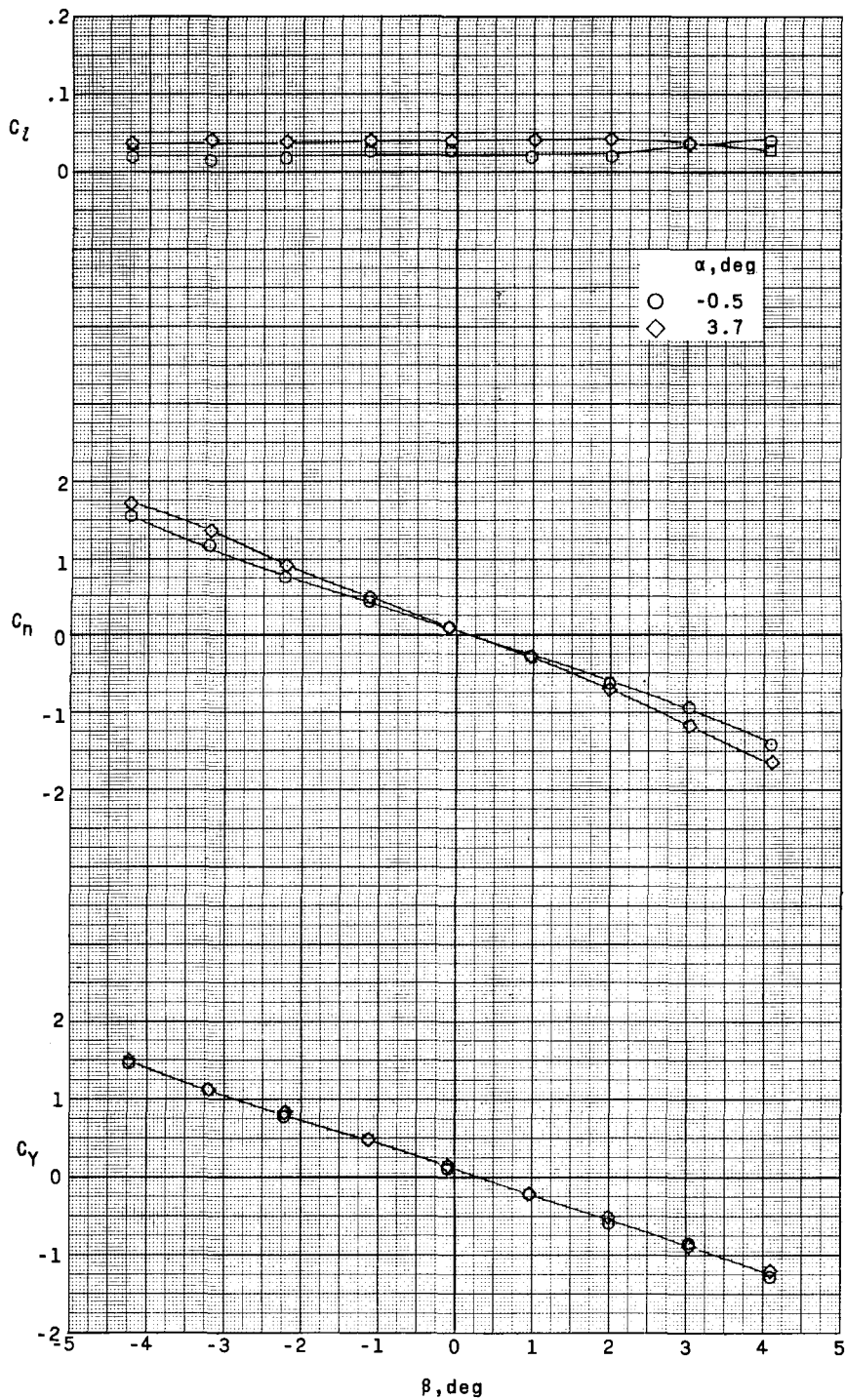
(a) $M = 1.80$; fins $F_1 F_3$; $\delta_I = \delta_{II} = 0^\circ$.

Figure 11.- Lateral aerodynamic characteristics of model 2 with four auxiliary rocket motors at several angles of attack.



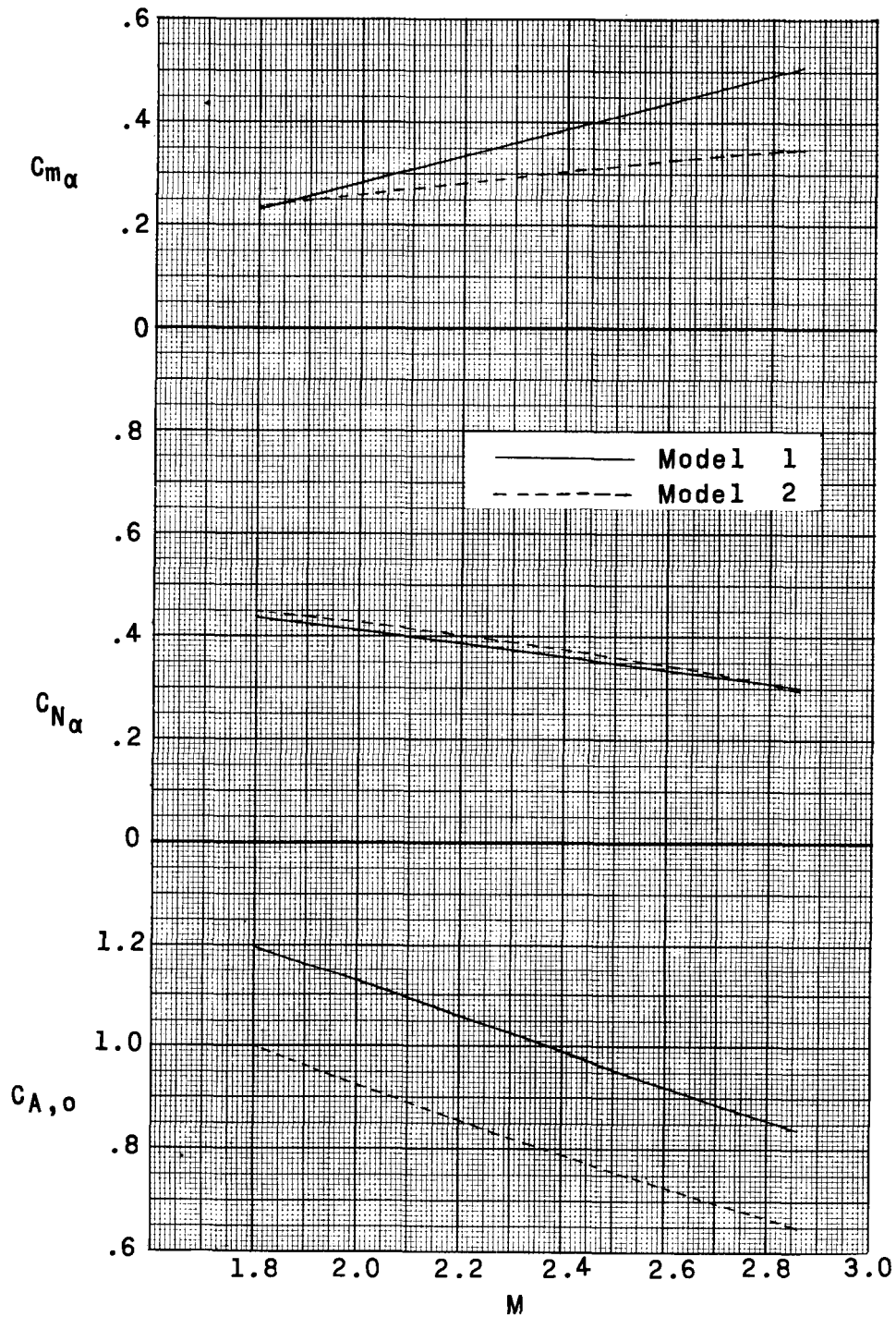
(b) $M = 2.50$; fins $F_1 F_3$; $\delta_I = \delta_{II} = 0^\circ$.

Figure 11.- Continued.



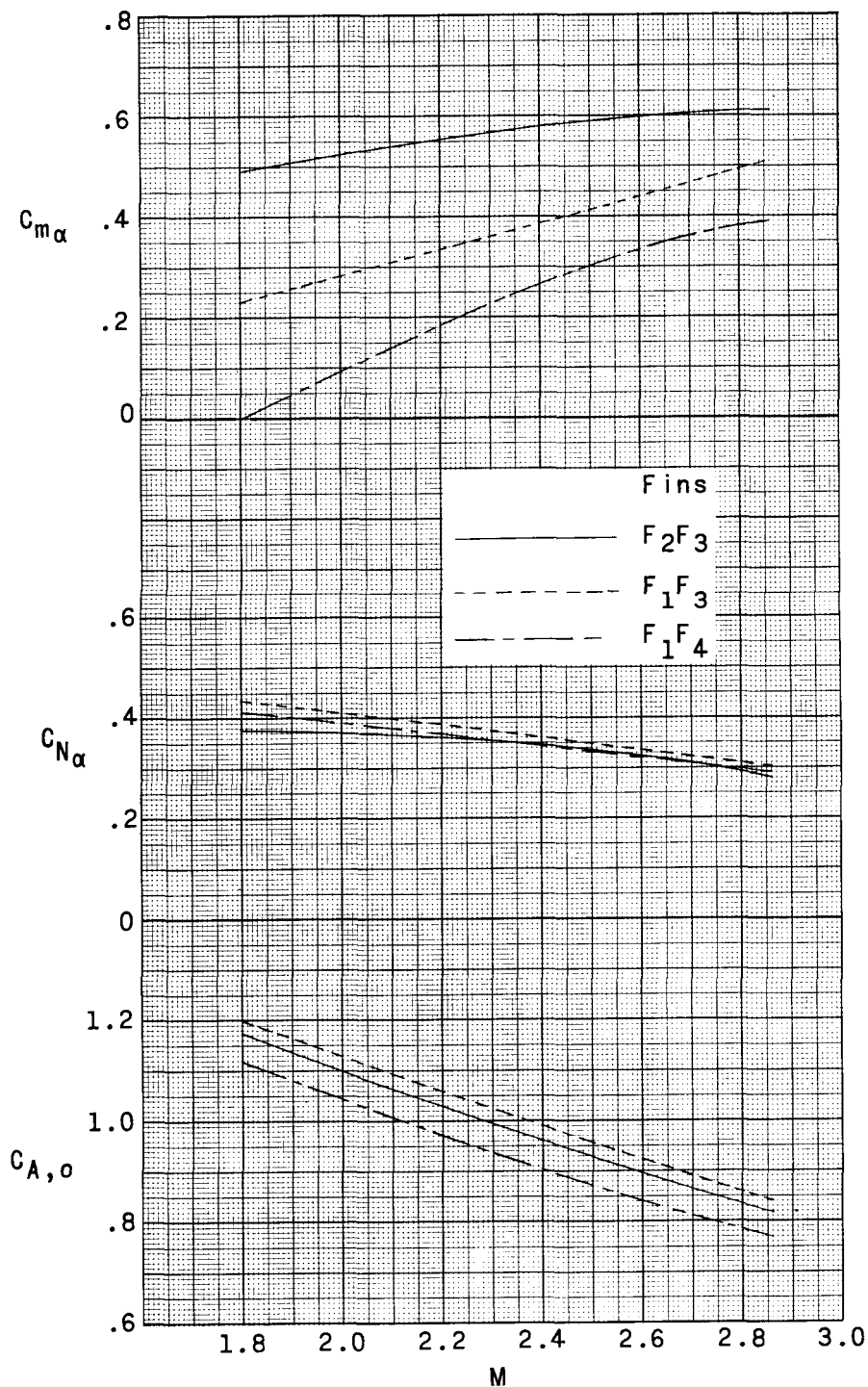
(c) $M = 2.86$; fins $F_1 F_3$; $\delta_I = \delta_{II} = 0^\circ$.

Figure 11.- Concluded.



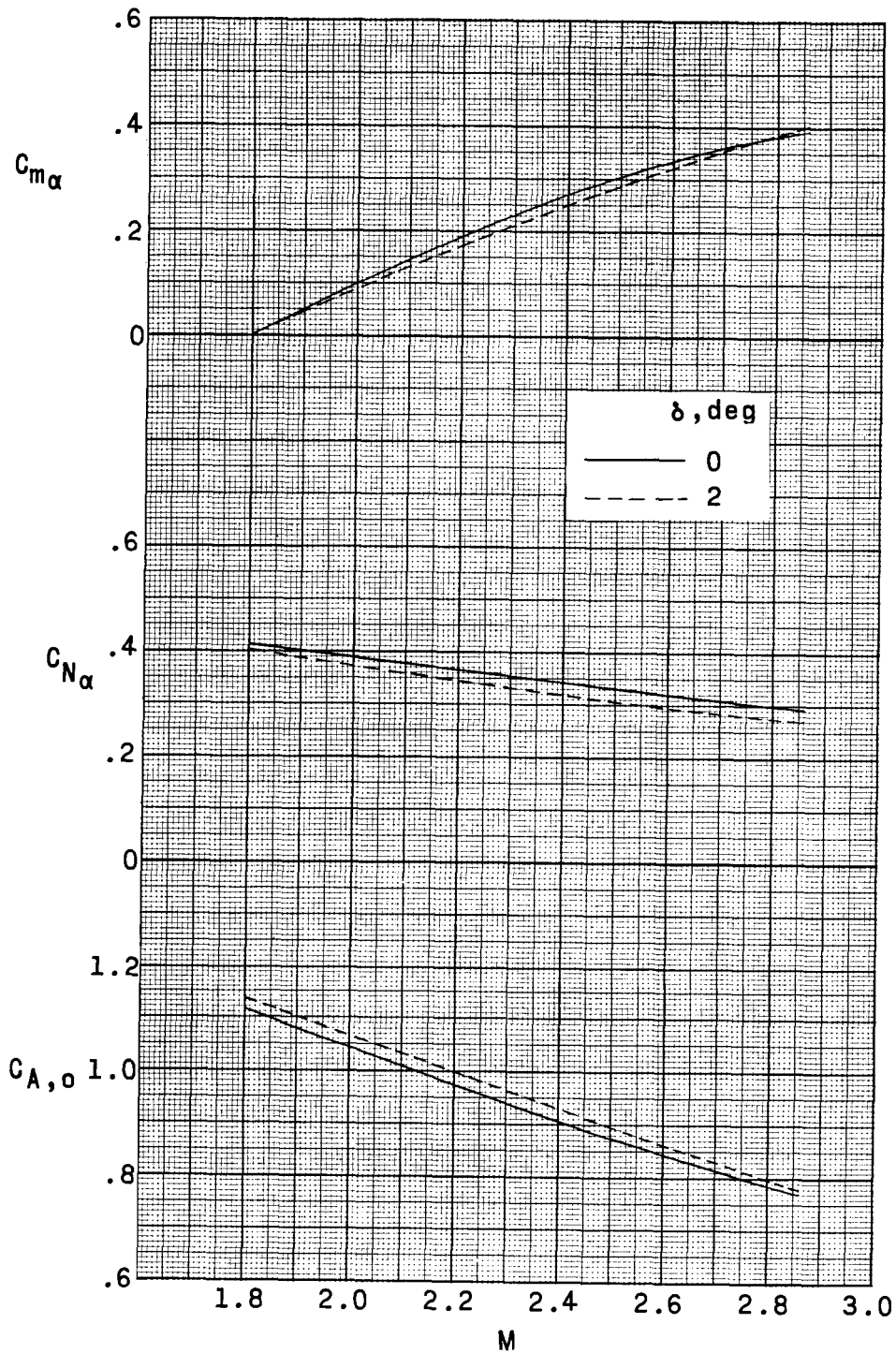
(a) Body effect. Fins F_1F_3 ; two auxiliary rocket motors; $\delta_I = \delta_{II} = 0^\circ$.

Figure 12.- Variation of longitudinal aerodynamic parameters with Mach number.



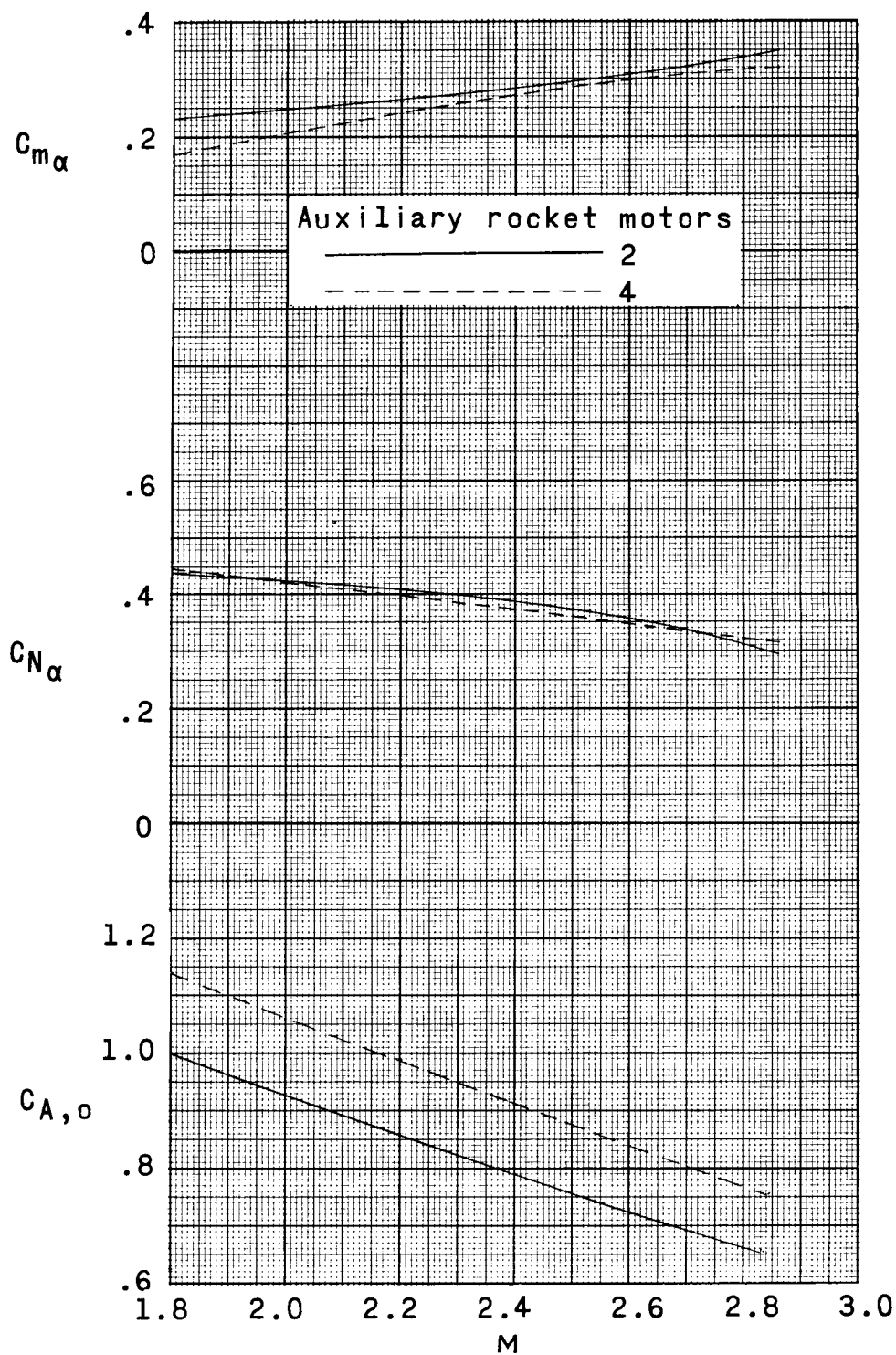
(b) Fin effect. Model 1; two auxiliary rocket motors; $\delta_I = \delta_{II} = 0^\circ$.

Figure 12.- Continued.



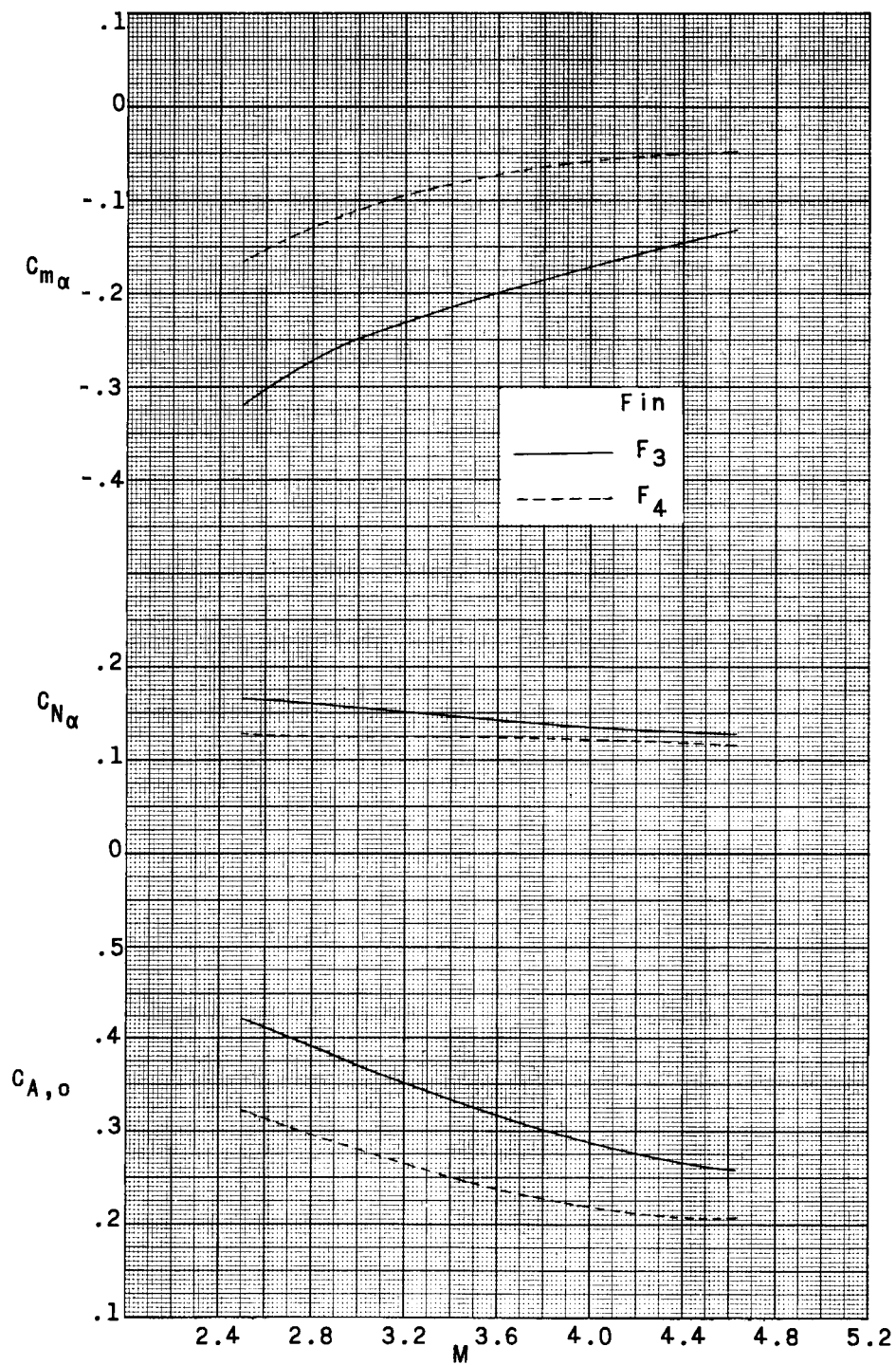
(c) Fin-cant effect. Model 1; fins F_1F_4 ; two auxiliary rocket motors.

Figure 12.- Continued.



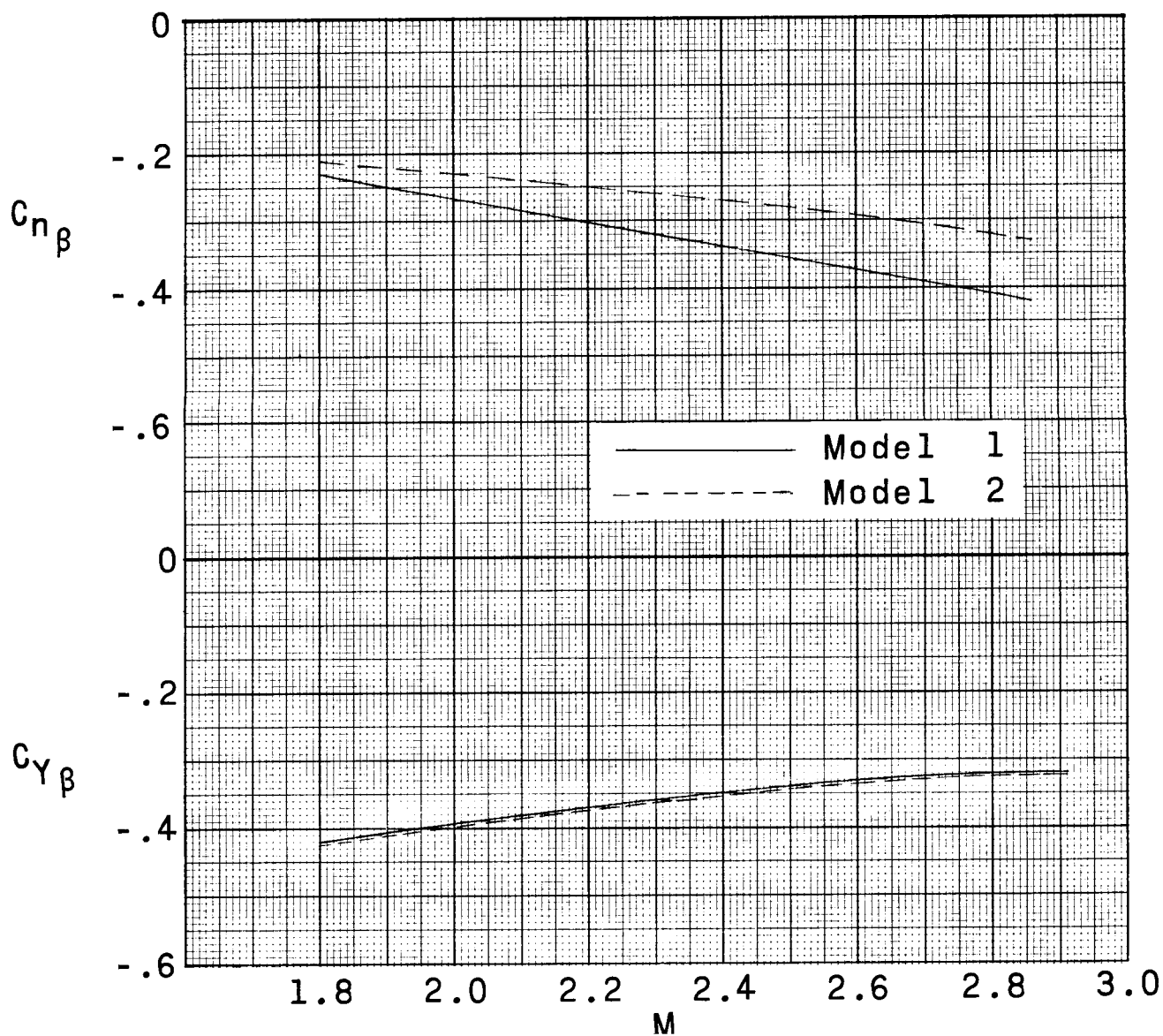
(d) Auxiliary rocket motor effect. Model 2; fins F_1F_3 ; $\delta_I = \delta_{II} = 0^\circ$.

Figure 12.- Continued.



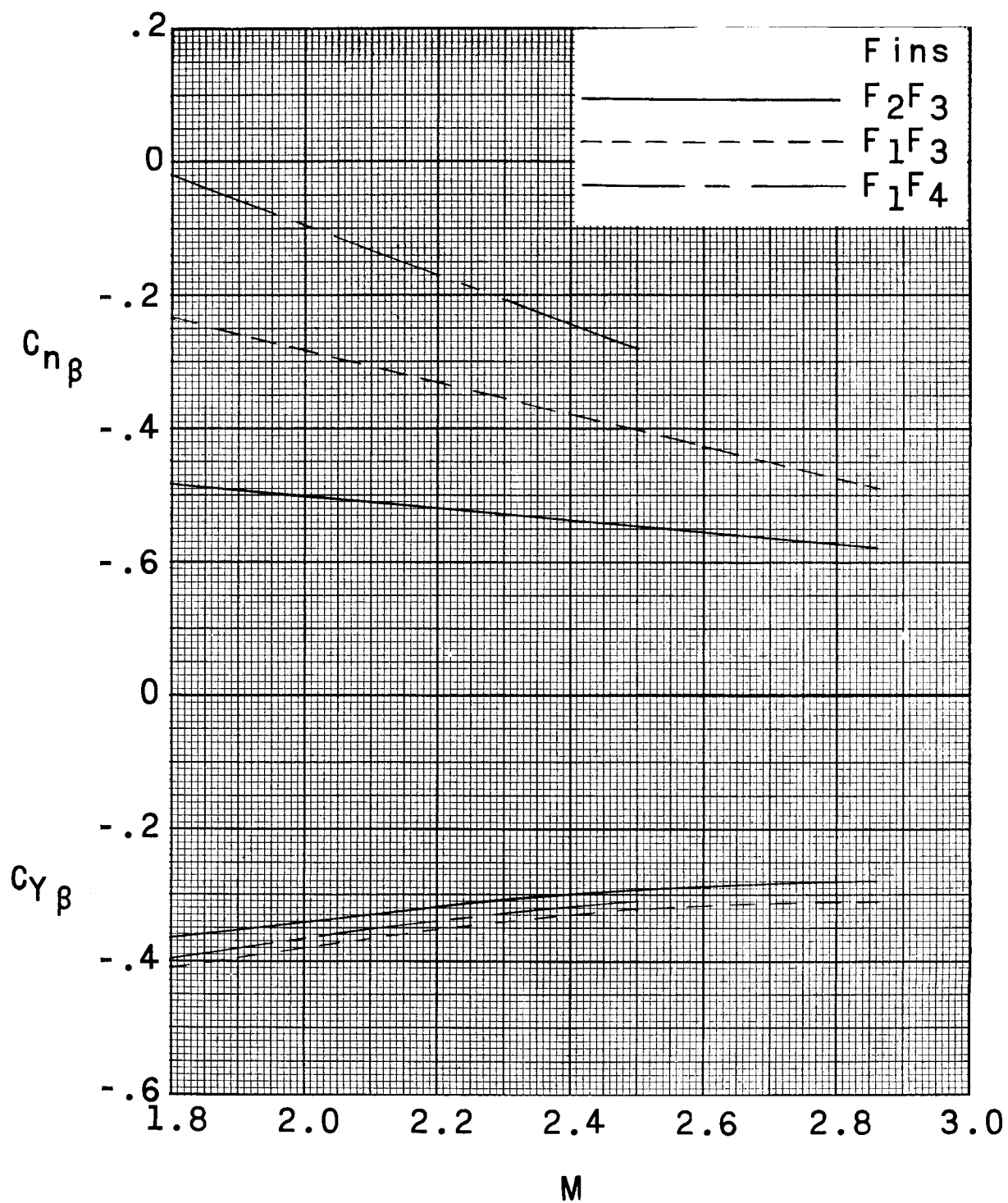
(e) Fin effect. Model 3; $\delta_I = 0^\circ$.

Figure 12.- Concluded.



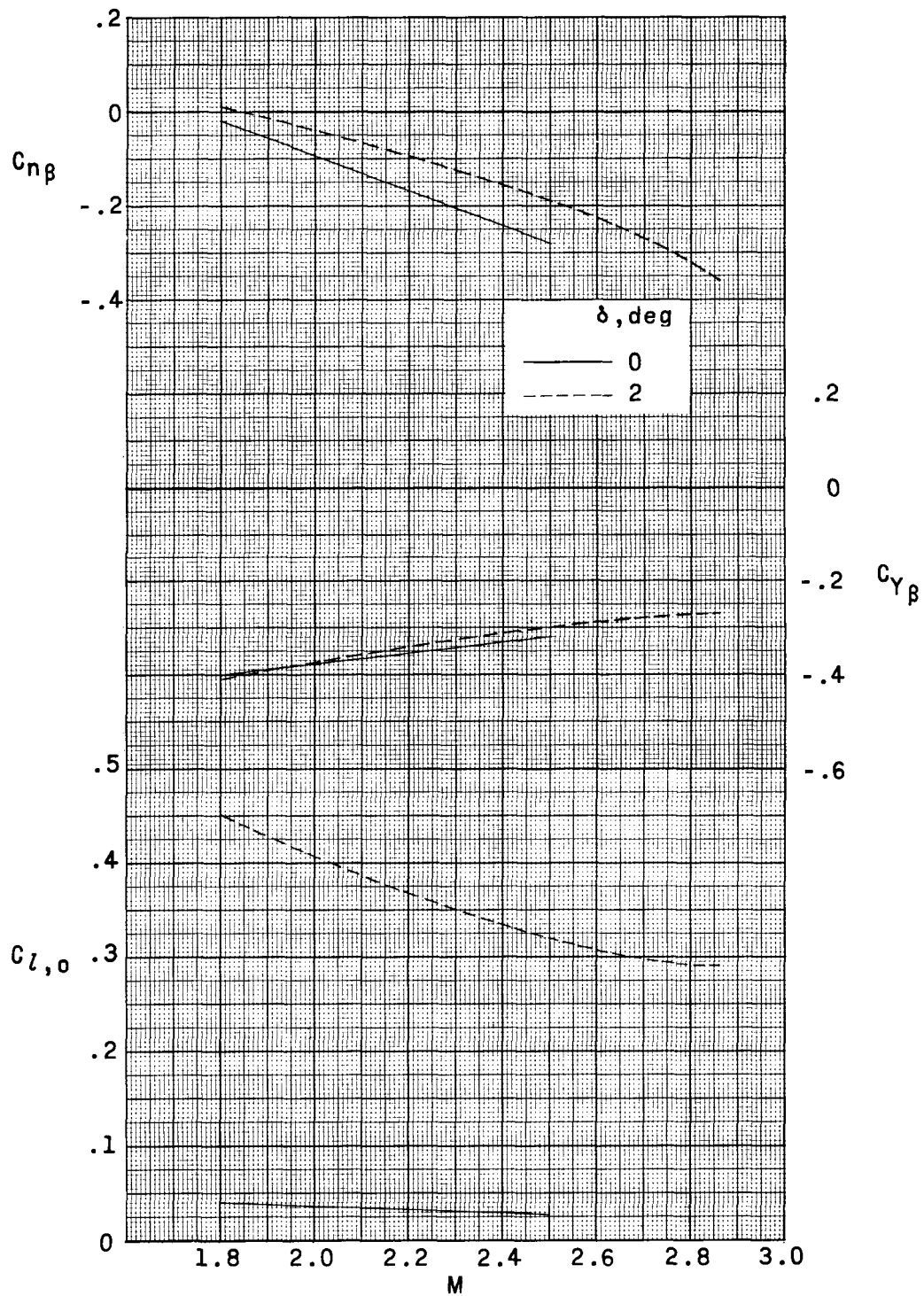
(a) Body effect. Fins $F_1 F_3$; two auxiliary rocket motors; $\delta_I = \delta_{II} = 0^\circ$.

Figure 13.- Variation of lateral aerodynamic parameters with Mach number. $\alpha \approx 0^\circ$.



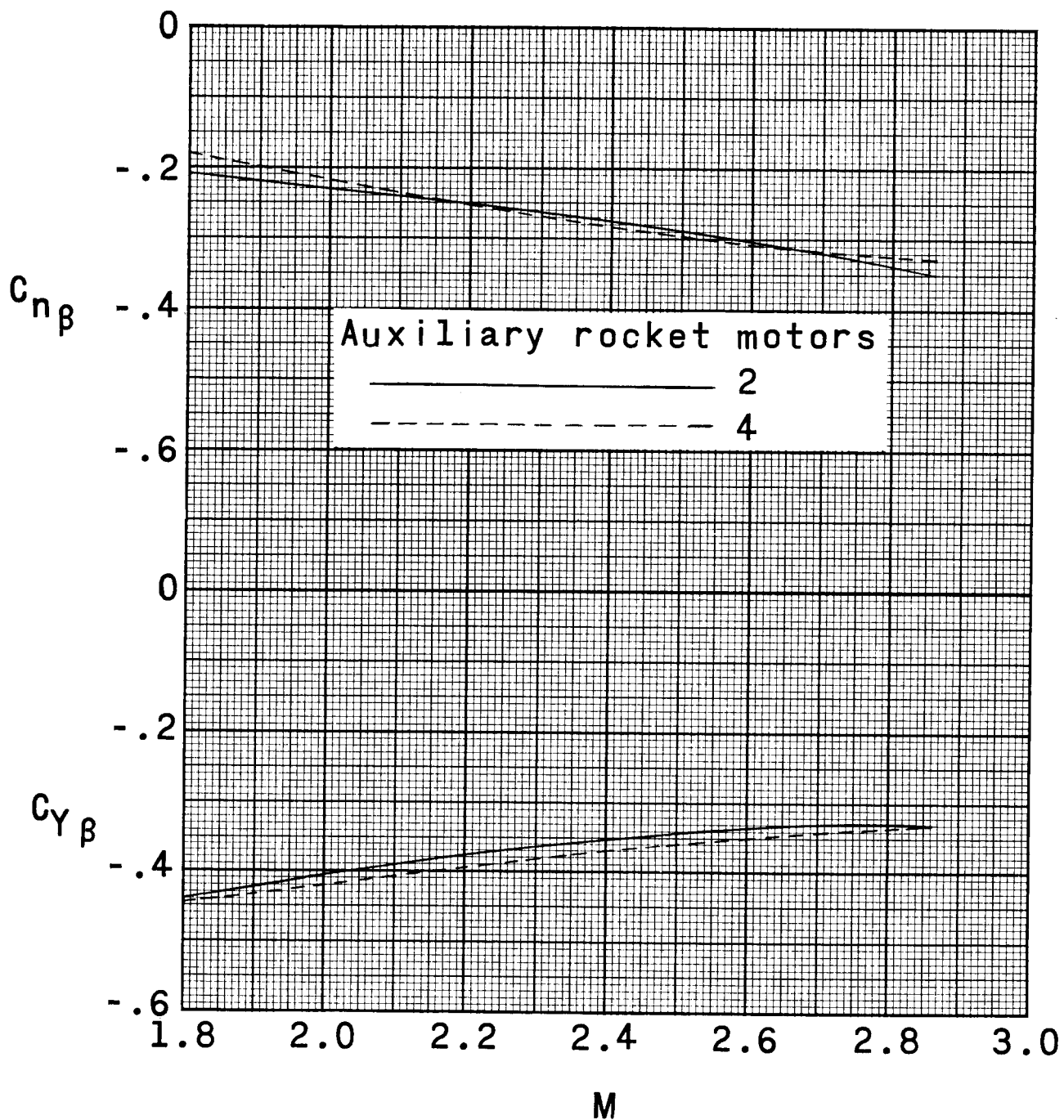
(b) Fin effect. Model 1; two auxiliary rocket motors; $\delta_I = \delta_{II} = 0^\circ$.

Figure 13.- Continued.



(c) Fin-cant effect. Model 1; fins F_1F_4 ; two auxiliary rocket motors.

Figure 13.- Continued.



(d) Auxiliary rocket-motor effect. Model 2; fins F_1F_3 ; $\delta_I = \delta_{II} = 0^\circ$.

Figure 13.- Concluded.